remote sensing

MDPI

Article

Soil Erosion Satellite-Based Estimation in Cropland for Soil Conservation

Bruna Cristina Gallo [1,2], Paulo Sérgio Graziano Magalhães [3], José A. M. Demattê [4,*], Walter Rossi Cervi [1,5], João Luís Nunes Carvalho [2], Leandro Carneiro Barbosa [2], Henrique Bellinaso [4], Danilo César de Mello [6], Gustavo Vieira Veloso [6], Marcelo Rodrigo Alves [7], Elpídio Inácio Fernandes-Filho [6], Márcio Rocha Francelino [6] and Carlos Ernesto Gonçalves Reynaud Schaefer [6]

1 Interdisciplinary Ph.D. Program in Bioenergy, University of Campinas, Campinas 13083-862, SP, Brazil
2 Brazilian Biorenewables National Laboratory (LNBR), Brazilian Center of Energy and Material Research (CNPEM), Campinas 13083-100, SP, Brazil
3 Interdisciplinary Center of Energy Planning, University of Campinas, Campinas 13083-862, SP, Brazil
4 Department of Soil Science, Luiz de Queiroz College of Agriculture, University of São Paulo, Piracicaba 13418-900, SP, Brazil
5 Wageningen Economic Research, Wageningen University & Research, 6708 PB Wageningen, The Netherlands
6 Department of Soil Science, Federal University of Viçosa, Viçosa 36570-900, MG, Brazil
7 Department of Environment and Regional Development, University of West São Paulo (UNOESTE), Rod. Raposo Tavares, km 572-Limoeiro, Presidente Prudente 19067-175, SP, Brazil
* Correspondence: jamdemat@usp.br

Abstract: Intensive cropland expansion for an increasing population has driven soil degradation worldwide. Modeling how agroecosystems respond to variations in soil attributes, relief and crop management dynamics can guide soil conservation. This research presents a new approach to evaluate soil loss by water erosion in cropland using the RUSLE model and Synthetic Soil Image (spectroscopy technique), which uses time series remotely sensed environmental, agricultural and anthropic variables, in the southeast region of São Paulo State, Brazil. The availability of the open-access satellite images of Tropical Rainfall Measuring Mission (TRMM) and Landsat satellite images provided ten years of rainfall data and 35 years of exposed soil surface. The bare soil surface and agricultural land use were extracted, and the multi-temporal rainfall erosivity was assessed. We predict soil maps' attributes (texture and organic matter) through innovative soil spectroscopy techniques to assess the soil erodibility and soil loss tolerance. The erosivity, erodibility, and topography obtained by the Earth observations were adopted to estimate soil erosion in four scenarios of sugarcane (*Saccharum* spp.) residue coverage (0%, 50%, 75%, and 100%) in five years of the sugarcane cycle: the first year of sugarcane harvest and four subsequent harvesting years from 2013 to 2017. Soil loss tolerance means 4.3 Mg ha^{-1} exceeds the minimum rate in 40% of the region, resulting in a total soil loss of ~6 million Mg yr^{-1} under total coverage management (7 Mg ha^{-1}). Our findings suggest that sugarcane straw production has not been sufficient to protect the soil loss against water erosion. Thus, straw removal is unfeasible unless alternative conservation practices are adopted, such as minimum soil tillage, contour lines, terracing and other techniques that favor increases in organic matter content and soil flocculating cations. This research also identifies a spatiotemporal erosion-prone area that requests an immediately sustainable land development guide to restore and rehabilitate the vulnerable ecosystem service. The high-resolution spatially distribution method provided can identify soil degradation-prone areas and the cropland expansion frequency. This information may guide farms and the policymakers for a better request of conservation practices according to site-specific management variation.

Keywords: soil degradation; RUSLE; remote sensing; crop residue; bioenergy; sustainable land use

Citation: Gallo, B.C.; Magalhães, P.S.G.; Demattê, J.A.M.; Cervi, W.R.; Carvalho, J.L.N.; Barbosa, L.C.; Bellinaso, H.; Mello, D.C.d.; Veloso, G.V.; Alves, M.R.; et al. Soil Erosion Satellite-Based Estimation in Cropland for Soil Conservation. *Remote Sens.* **2023**, *15*, 20. https://doi.org/10.3390/rs15010020

Academic Editor: Xianjun Hao

Received: 19 October 2022
Revised: 7 December 2022
Accepted: 12 December 2022
Published: 21 December 2022

1. Introduction

One-third of global land is occupied by livestock (21%) and agriculture (12%) [1]. The increasing demand of a growing population projected to reach 9.6 billion by 2050 from the current 7.7 billion [2] has put the pressure on the Earth's land for food, natural resources, and climate change and created new challenges between humanity and the world's fertile soil resources.

Soil erosion rates caused by the immense expansion of cropland areas have exceeded the rate that soil is formed by one to two orders of magnitude [3]. The process of soil erosion usually involves the detachment, breakdown, transport, redistribution and deposition of sediments [4]. Soil erosion globally has resulted in around 25 to 40 billion tons of increased sediment every year [2]. Land-use change to cropland is responsible for ~80% of the erosion increase. The highest soil erosion occurs in the least developed countries due to the accelerated soil erosion driven by land-use change and poor land management. On the other hand, these countries have the highest potential of soil erosion reduction by conservation agriculture adoption [5].

Sustainable land management (SLM) is treated as an effective land degradation reduction method to achieve the Sustainable Development Goals (SDGs) regarding food, health, water, climate, and land management [6]. SDGs are a global call to end hunger and poverty, protect the planet, and ensure peace and poverty for all by 2030. Despite the SLM's importance for land and soil degradation, identifying large soil management scaling areas in space and time is challenging due to the time-consuming and high cost for data acquisition of the complex climatic, abiotic ecological factors (i.e., soil characteristics and topography), type of land use and land management practices (i.e., tillage and crop rotation). Land-use change does not occur linearly over time, since land rights vary in places and are dependent on the political–economic and legal situation [7].

The Universal Soil Loss Equation (USLE) [8] and its revised version (RUSLE) [9] are the most used empirical models to estimate soil erosion driven by water globally. It aims to guide conservation planning and supports the planners to evaluate and predict the soil erosion rate for each of several alternative combinations of cropping systems and management techniques on any site within the specified limits. The RUSLE equation integrates erosivity, erodibility, topography, cover management, and support practice factors. Furthermore, it considers soil loss tolerance, which ponders the productivity loss due to erosion with the rate of soil formation from parent material, the role of topsoil formation, loss of nutrients and the cost to replace them [9].

Remote Sensing (RS) linked with Geographic Information System (GIS) combined in RUSLE provide data to compute soil erosion with better spatial coverage and accuracy with reasonable costs [10]. The soil spectroscopy advent overcomes the lack of reliable soil data that can be applied to the least developed economies. This method along with the Earth observation-based data can be used to assess the soil erodibility factor based on the environmental soil service (organic matter and mineral composition) with the spectral reflectance data [10,11].

Southeast Brazil is the core of sugarcane production with about 5 million hectares in the 2019/2020 season (62% of the national production) [12]. It was estimated that 600 million Mg yr^{-1} of annual rainfall soil erosion loss occurs annually in this region [13]. Sugarcane crop in southern Brazil requires a large amount of land to produce biofuels, sugar and electricity. In general, sugarcane production is based on conventional tillage using green mechanized harvesting every year, with a replanting period every five years. The transition from a burned to green harvest system resulted in the maintenance of a large amount of sugarcane straw on the soil surface [14]. The thick layer of straw (ranging from 10 to 20 Mg tons ha^{-1}) covering the soil after harvesting resulted in several benefits, such as nutrient cycling [15], carbon storage [16], better soil physical and biological conditions [17,18] and control against erosion processes [19]. However, although straw covers results in several ecosystem benefits, Brazil's more recent sugarcane sector has

shown interest in removing part of this crop's residue for bioenergy production, which would lead to increased soil degradation in sugarcane fields [20].

There is a tenuous line between soil degradation and sustainable land management in cropland. In sugarcane fields, straw is an essential source of soil conservation because it benefits soil functioning, e.g., erosion protection cover, soil temperature amplitude reduction, and biological activity increasing [21]. Studies have demonstrated that maintaining 7 to 10 Mg tons ha^{-1} of straw is enough to cover 100% of the area prevailing the crop's agronomic benefits [22,23]. It suggested that if the straw yield exceeds this amount, it may be used as feedstock for Brazil's bioenergy demand (bioelectricity and cellulosic ethanol).

This paper presents a new approach to evaluate spatial and temporal patterns of soil loss and the impacts of straw removal in the southeastern part of Brazil by integrating environmental variables with the cropland management dataset, field data, RS and GIS data in the RUSLE model. A modern multi-temporal satellite-based estimation method was conducted to assess the soil proprieties and spatial patterns of agricultural land use over the last three decades as well as rainfall data in the last decade. Four soil loss scenarios have been assessed by simulation with four different straw coverage rates of about 0, 50, 75 and 100%, respectively, in five years of the sugarcane cycle (2013–2017) to enlighten the impacts of straw removal changes on soil erosion.

The main novelties of this research are related to the soil erodibility parameters of RUSLE and the soil loss tolerance obtained by the soil attribute maps (texture and organic matter) through the bare soil spectroscopy technique (Synthetic Soil Image). This method combines a Revised Universal Soil Loss Equation (RUSLE) model associated with a time series remotely sensed data to estimate soil loss by water erosion in cropland.

2. Materials and Methods

2.1. Site Description and Sugarcane Cycle

We evaluate the soil erosion of 500 km^2 of agricultural sugarcane land-use area located in the southeastern part of Brazil, west of São Paulo State (Figure 1a). The erosion processes in this region may deliver sediments to the nearby rivers. Therefore, we expanded soil erosion estimations into 13 sub-basins (~1600 km^2) based on the streamflow in order to have a multi-perspective overview of the possible off-site effects of soil erosion on the hydrological ecosystem (Figure 1a).

The region is classified as tropical with dry winter (May–September). The average annual rainfall is 1391 mm yr^{-1}, and the average annual temperature is 24 °C [24]. The landscape is gently undulating and rolling uplands, with slopes ranging between 0 and 28%. The predominance of sandy–mudstone parental material [25] characterizes the soils' sandy/loam texture dominance. Sheet and interill are preponderating types of erosion in the study site (Figure 1b), but gully erosion sites are common, especially in ascending terrain (Figure 1c).

The sugarcane cycle comprises five years: the plant cane harvest and four subsequent harvesting years (ratoons) (Figure 2). Conventional tillage operations are the most common practices during the plant cane stage and the replanting period, which lies in glyphosate application, subsoiling, plowing, harrowing with physical, chemical, and or biological corrections. Conventional tillage is the most critical period due to the exposed soil period until the crop canopy closure (three to six months later) causing erosion. In areas cultivated with sugarcane, the main attributes of the terrain that contribute to erosion are extreme weather events such as the high intensity and volume of rainfall and soil exposure associated with sloping reliefs. So, the harvest period occurs every year or 18 months, and the maintenance of the straw in the field reduces the risk of soil erosion at this step.

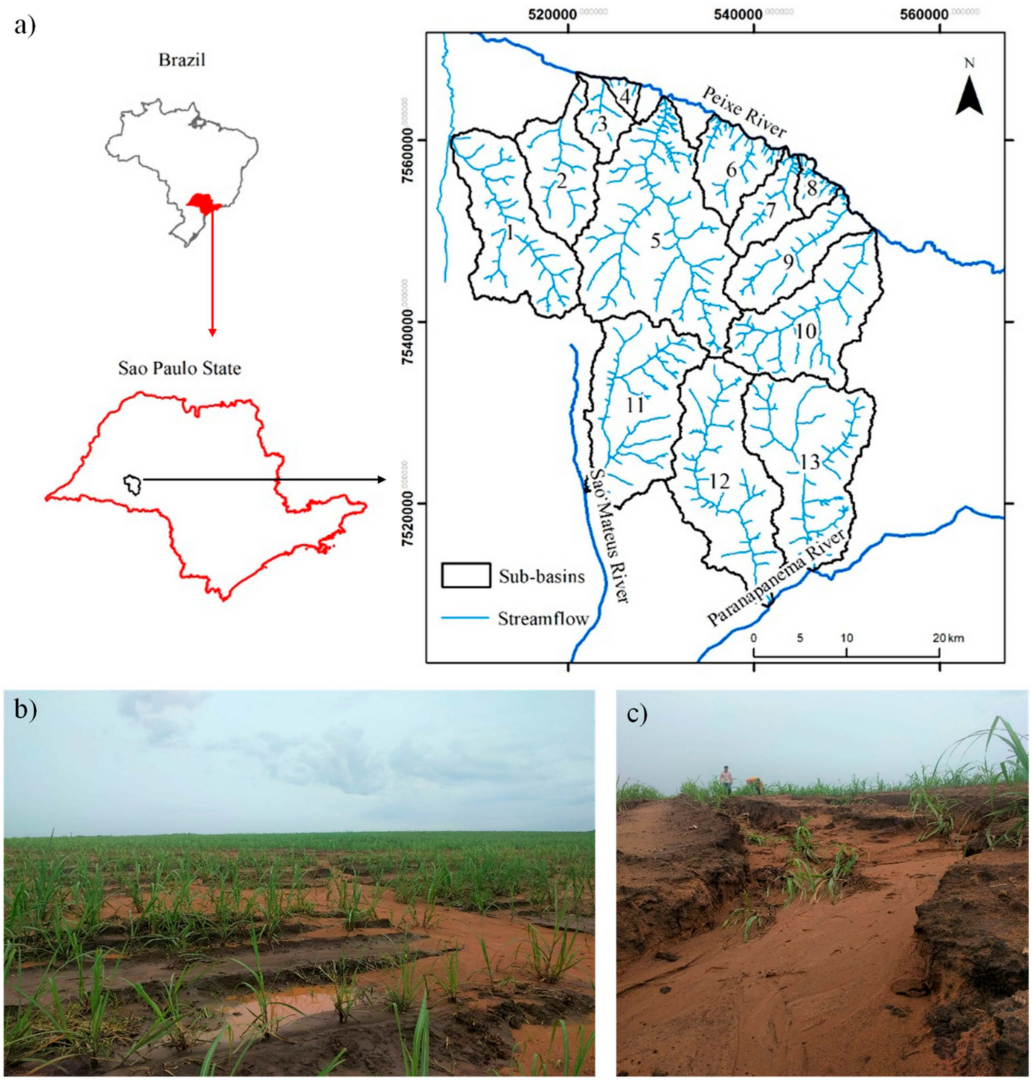

Figure 1. (**a**) Study location, (**b**) sheet and interrill erosion process and (**c**) gully erosion development during the rainy season at the beginning of the plant cane harvest under conventional tillage.

2.2. Soil Sampling

Sixty-seven topsoil (Epipedon) samples were collected randomly; 20% of the soil samples validated the soil erodibility maps generated from remote sensing. The soil samples brought to the laboratory were oven-dried for 48 h at 50 °C; then, they were ground and sieved (2 mm mesh) to analyze the soil organic carbon and particle size properties according to [26]. The main soil classes found in the study site, according to the World Reference Base for Soil Resources (WRB) [27] were Gleysols, Ferralsols, Lixisols, Leptosols and Arenosols.

2.3. Parametrization of Soil Loss by Water Erosion

Multi-temporal satellite image and field observations assessment provide soil loss estimation. Figure 2 demonstrates the general flowchart of the methodology to obtain soil loss.

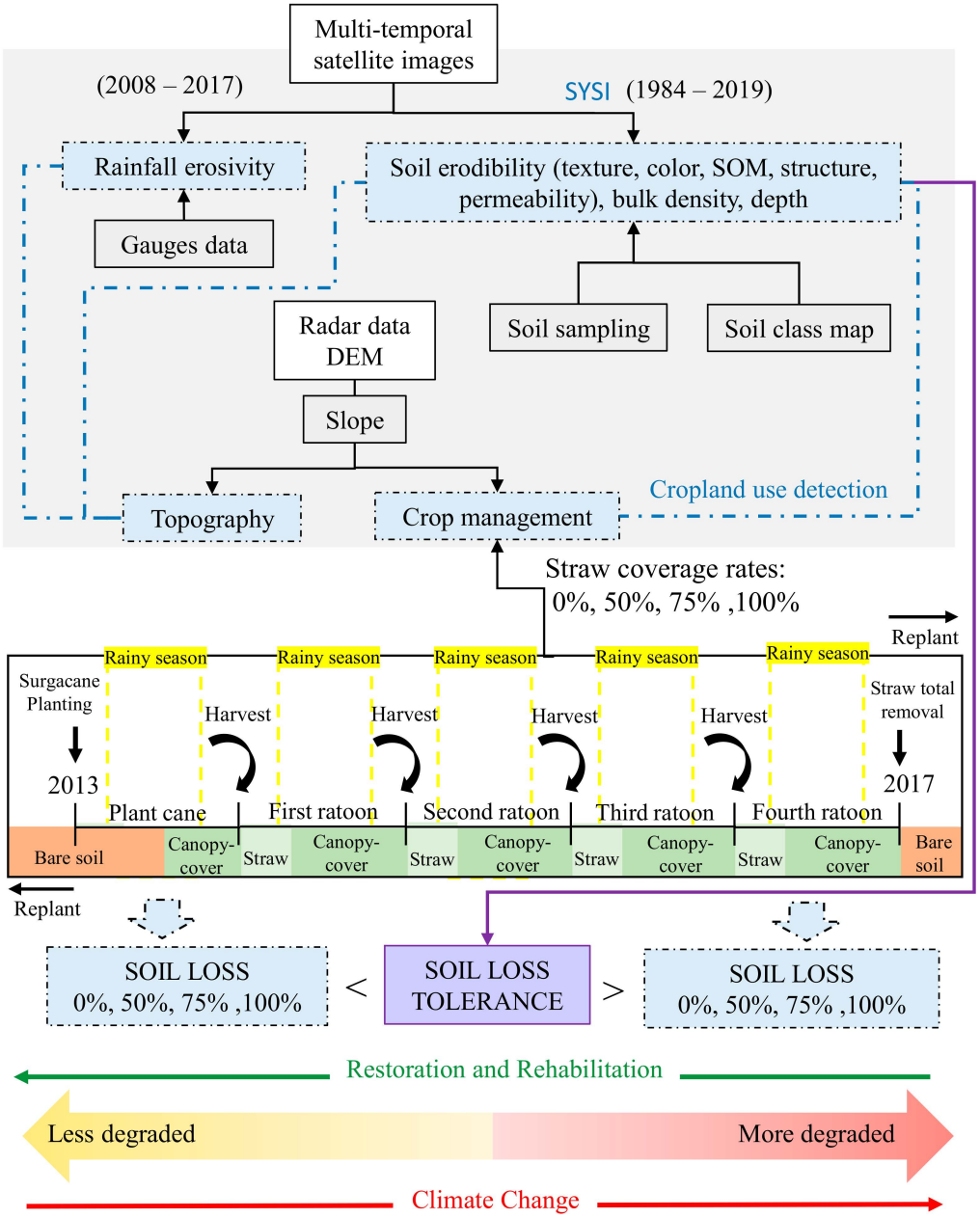

Figure 2. Flowchart of the methodology to obtain soil loss. The multi-temporal satellite image and field observations data used to estimate and validate rainfall erosivity and soil erodibility, and a digital elevation model used to derive the slope. The Synthetic Soil Image (SYSI) technique based on remote sensing and soil spectroscopy-derived soil attributes maps to calculate soil erodibility, soil loss tolerance and detect the cropland use spatial patterns. The environmental variables (rainfall, erodibility and topography) associated with the cropland patterns and the cropland management dataset (five years of the sugarcane cycle) under different amounts of straw (0%, 50%, 75%, and 100%) estimate soil loss. Soil loss higher than the tolerance indicates high land degradation that contributes to increasing climate change crises, while lower indicates the restoration and rehabilitation of the ecosystem.

The Revised Universal Soil Loss Equation (RUSLE) (Equation (1)) [28] implemented in Geographic Information System (GIS) was used to assess the soil erosion rate (Table 1 and Figure 1). Soil losses by water erosion refer to the amount of sediment that reaches the end of a specified area (cell) on a hillslope [5]. Using a GIS raster scheme means that each cell is independent of the others. Thus, soil erosion is not routed downslope across each

cell from hillslopes to the sink area or the riverine systems. The RUSLE model does not capture gullying and other geomorphic processes (i.e., mudflows, landslides and tillage erosion) [29]. However, it indicates the soil loss rate at which gully erosion might be expected to begin [9].

$$\text{Soil Loss} = R * K * LS * C * P \quad (1)$$

Table 1. Synthesis of the RUSLE spatial dataset required to map soil loss by water erosion.

Factor	Environmental Dataset	Tools/Method	Variability	Spatial Dataset	Resolution/ Map Scale
Rainfall (R-Factor)	Average Monthly/ Annual Rainfall	Google Engine, Literature/MFI [1]/EI_{30} [2]	Spatiotemporal (10 years)	TRMM [3]	25 km
Soil (K-Factor)	Texture, Organic matter, Bulk density	Google Engine/SYSI [4] and R program/DSM [5]	Spatiotemporal (35 years)	Landsat	30 m
	Permeability and Structure code	Legacy Soil Maps	Shape	Region Map Local Soil Map	1:250,000 1:50,000
Topography (LS-Factor)	Slope, Flow direction, Flow accumulation	ArcGIS	Spatial	SRTM [6]	30 m
Management (P-Factor)	Slope and Contour farming	ArcGIS	Spatial	SRTM [6]	30 m
(C-Factor)	Land use	Google Engine/SYSI [4]	Spatiotemporal (35 years)	Landsat	30 m
	Canopy cover, Surface cover, Surface roughness, Soil moisture	Excel/Sugarcane management combinations [7]	Shape (5 years)	Cropland plots	1:50,000

[1] MFI: Modified Fournier Index, [2] EI30: Erosivity Index, [3] TRMM: Tropical Rainfall Measuring Mis-sion, [4] SYSI: Soil Synthetic Image, [5] DSM: Digital Soil Map, [6] SRTM: Shuttle Radar Topographic Mission, [7] Local, Planting and Tillage Date, Tillage System, Crop Rotation, Straw Management, Sugarcane Cycle, and Management Levels.

The detachment-limited model outputs the mass of soil lost per unit area and time (Mg ha^{-1} yr^{-1}). Sheet, interrill and rill erosion processes are given by the multiplication of six parameters: rainfall erosivity (R-Factor in MJ mm^{-1} h^{-1} y^{-1}), soil erodibility (K-Factor in tons. h. MJ^{-1} mm^{-1}), slope length (L-Factor in meters), slope steepness (S-Factor in percentage), cropping system (C-Factor), and erosion control practice (P-factor). C and P-factors are dimensionless (Table 1). The spatial resolutions range from 30 m to 25 km, and the parameters were resampled to a 30 × 30 m cell size to model soil loss as the final output.

The soil loss tolerance threshold (T-value) indicates the maximum rate of soil erosion that can occur and still permits crop productivity to be sustained economically [8,9]. The T value according to [30] is estimated by: (1) soil thickness; (2) soil formation rate; (3) guidelines of the USDA-NRCS; and (4) productivity index. In addition, the T value for a specific soil is a function of the following: the rate of soil formation from parent material; the rate of topsoil formation from subsoil; reduction in crop yield by erosion; soil depth; changes in soil attributes favorable for plant growth; loss of plant nutrients by erosion; the likelihood of rill and gully formation; sediment deposition problems within a field; sediment delivery from the erosion site and; and the availability of feasibility, economically, culturally and socially in addition to soil conservation practices [30]. Cropping management practices with the predicted soil loss rate less than the T-value rate may be projected to deliver less soil degradation (Figure 2). Thus, sustainable land management practices can reduce the risk of land degradation and mitigate the climate change impacts by promoting the restoration and rehabilitation of the ecosystems, for example, by improving their carbon stock [1].

2.3.1. Rainfall Erosivity Factor (R)

Rainfall erosivity represents the erosive powers of rainfall energy (intensity and duration), a total of rain (volume) and frequency over extended time events. We calculated the R-Factor using ten years (2008–2017) of data of the monthly 3B42 product from the Tropical Rainfall Measuring Mission (TRMM) Multi-satellite Precipitation Analysis (TMPA). Several studies worldwide have estimated erosivity at fair resolution using the TRMM [11,31,32].

This product provides global coverage of precipitation (mm hr^{-1}) with a 3 h temporal resolution and a 0.25 degree spatial resolution [33].

We performed the Modified Fournier Index (MFI) (Equation (2)) using TRMM products to estimate the erosivity factor according to the Erosivity Index (EI_{30}) equations recommended by [34,35]. The EI_{30} is defined as the product of the maximum rain intensity during a 30 min period. There are three main stations relating EI_{30} to MFI that fit the study site location (Table 2). Our calculated R-Factor is an average of the three erosivity equations. We used data from seven gauges provided by the Water and Electric Energy Department of São Paulo State (DAEE-SP) located toward the study site to validate the R-Factor obtained from TRMM.

$$\mathrm{MFI} = \frac{1}{\mathrm{P}} \sum_{\mathrm{i}=1}^{12} * \mathrm{Pi}^2 \quad (2)$$

Table 2. Erosivity equations studies around the study site.

Latitude	Longitude	City/State	Equation	Authors
22°37′0″S	52°10′0″W	Teod. Sampaio/SP	EI_{30} = 106.82 + 46.96 (MFI)	[36]
22°31′12″S	47°2′40″W	Campinas/SP	EI_{30} = 68.73 (MFI) $^{0.841}$	[37]
23°13′0″S	49°14′0″W	Piraju/SP	EI_{30} = 72.55 (MFI) $^{0.8488}$	[38]

EI_{30}: Erosivity Index and MFI: Modified Fournier Index.

P is the average annual rainfall (mm), and Pi is the average rainfall (mm) in the month i.

2.3.2. Soil Erodibility Factor (K)

The soil erodibility factor [28] represents soil susceptibility to erosion. The soil particle size distribution (clay, fine sand, and silt contents), soil organic matter (SOM) content, soil structure, and profile permeability are the attributes required to estimate the K-Factor [27] (Equation (3)) [8].

$$\mathrm{K} = [2.1 * 10\ \hat{}\ (-4) * \mathrm{M}\ \hat{}\ 1.14\ (12 - \mathrm{OM}) + 3.25\ (\mathrm{S} - 2) + 2.5\ (\mathrm{Q} - 3)/100] * 0.1317 \quad (3)$$

M = (% silt + % fine sand) ∗ (100 − % clay). OM is soil organic matter content (%). S is soil structure code (1–4). Q is permeability code (1–6).

Here, the topsoil attributes were spatially modeled using an improved methodology with satellite Bare Soil Composite Image [39] based on a Geospatial Soil Sensing System data-mining algorithm. This algorithm flagged bare surfaces from the collection of historical images and aggregated the spatially bare soil fragments into a synthetic soil image (SYSI) [40–42]. In this study, we used multi-temporal Landsat satellite images to extract bare soil fragments from 1984 to 2019 and aggregate them in order to obtain all periods of exposed soil for the later creation of a mosaic, which allows viewing the entire area of interest with an exposed soil surface. Landsat imagery has the wavelengths (Bands) of Visible (VIS—Blue/Green/Red), Near Infrared (NIR) and Shortwave Infrared (SWIR1 and SWIR 2) with 30 m of spatial resolution and 16 days of temporal resolution.

MID-Infrared and NDVI indexes were used to remove vegetation and crop residue in each image. We used quality bands to mask clouds and shadows. MID-Infrared represents the normalized difference index calculated from Landsat bands SWIR1 and SWIR2, and NDVI defines the normalized difference vegetation index calculated from Landsat bands NIR and Red. MID-Infrared and NDVI threshold combinations of −0.25 to 0.25 and 0.013 to 0.10. The indexes threshold was determined based on studies related to soil reflectance [40,42] and field observation. We used quality bands to mask clouds and shadows or pixels with inconsistent values, and we choose a filter to use Landsat images with no clouds. The images were aggregated into a single image by the median spectral reflectance value achieving the SYSI of the agricultural spatial patterns from a time interval

of 1984 to 2019, with a native spatial (30 m) Landsat product. We used the Google Earth engine platform to acquire the SYSI algorithm.

We performed a partial least square regression (PLSR) method to predict the digital soil mapping attributes by inputting the multi-temporal spectra data from the SYSI and the field measured soil samples (80% employed for calibration and the remaining 20% for validation) at the R program. The models were evaluated based on the coefficient of determination (R^2) and the root means square error (RMSE).

2.3.3. Slope Length and Steepness Factor (LS)

The LS-Factor [28] describes the effect of the topography on soil erosion. The L-Factor calculates the slope length, and the S-Factor measures the slope steepness. The L-Factor represents the distance from the overland flow point of origin to the point where the slope gradient decreases, water runoff is streamed into a channel and deposition starts [8,43].

Ref. [44] identify that the S-Factor is not uniform for a whole area; hence, they proposed sub-dividing the slope into several segments. Later, [45] extended this approach to a two-dimensional terrain using the unit-contributing area model (Equations (4)–(6)). Ref. [9] incorporated this approach into RUSLE with slope gradient concepts of [46], and they found that soil loss arises faster in slopes that were steeper than 9% (Equations (7) and (8)).

The LS-Factor was derived from a Digital Elevation Model (DEM) product obtained from the Topodata [44], which filled the original Shuttle Radar Topographic Mission (SRTM) 3 arc-second (90 m) data into an interpolated DEM of 1 arc-second (30 m). We calculated the slope length and slope steepness factors at the ArcGIS platform according to [9,45].

$$L_{i,j} = \frac{\left(A_{i,j-i,n} + D^2\right)^{m+1} - \left(A_{i,j-i,n}\right)^{m+1}}{\left(D^{m+2}\right) * \left(x_{i,j}{}^{m}\right) * (22.13)^{m}} \quad (4)$$

$$m = \frac{\beta}{\beta + 1} \quad (5)$$

$$\beta = \frac{\frac{\sin\theta}{0.0896}}{[0.56 + 3 * (\sin\theta)^{0.8}} \quad (6)$$

$$S = 10.8 * \sin\theta + 0.03, \text{ where slope gradient} < 0.09 \text{ ou } 9\% \quad (7)$$

$$S = 16.8 * \sin\theta - 0.5, \text{ where slope gradient} \geq 0.09 \quad (8)$$

$L_{i,j}$ is the slope length factor for the grid cell with coordinates (i, j). $A_{i,j}$ is an upslope contributing area for the grid cell with coordinates (i, j) (m^2). D is the side length of the grid cell (m). $x_{i,j}$ is a contour length coefficient for the grid cell with coordinates (i, j). m is related to the ratio β of the rill to interill erosion. θ is a gradient of slope in degrees. S is the slope steepness.

2.3.4. Control Practice Factor (P)

The P-Factor measures the ratio of soil loss expected for a specific support conservation practice to the corresponding loss with surface upslope and downslope tillage. The support practices for erosion control usually comprehend contouring, strip-cropping, terracing, and subsurface drainage. These practices influence drainage patterns, runoff velocity, and the direction of water volume concentration [9].

The cropland of the study site mainly applies contour farming in terraces according to the slope gradient. Contour means that farmers implement field practices along contours perpendicular to the normal water flow direction. Consequently, it reduces runoff velocity by increasing the surface roughness, providing more time for infiltration [47], protecting the fertile layer, improving crop yield, increasing income and contributing to the environment. The slope (%) (Table 3) was obtained by the DEM (30 m) derived P-Factor for the arable cropland.

Table 3. P-Factor for contour support practices for different slope gradients [8].

Slope (%)	P-Factor for Contouring
1–2	0.6
3–8	0.5
9–12	0.6
13–16	0.7
16–20	0.8
21–25	0.9
>25	0.95

2.3.5. Cover Management Factor (C)

The C-Factor comprises the effect of cropping and management practices on soil loss rates; this factor indicates how the management activities will affect the average annual soil and how the soil erosion potential will be disseminated in time during a conservation plan. The C-Factor value for a particular land use type is the weighted average of Soil Loss Ratios (SRLs) that ranges from 0 to 1 [9]; as it increases to 1, land use degradation stresses high soil threatens. The C-Factor may cause a considerable influence on the erosion calculation, which is defined as the most significant among the RUSLE factors [48].

We used a tool developed for sugarcane crops based on São Paulo State [49], and we calibrated it with the sugarcane stalks yield data from the agroindustry plots from 2013 to 2017. This tool enables many combinations of sugarcane system management as input data to obtain SLR subfactors (Equation (9)) and to model the average annual C-Factor (Equation (10)). It requires geographic location, date of tillage (month), tillage growing (winter, year or 18 months), tillage type (conventional, minimum or no-tillage), covers crop (bare soil, bare fallow, and green crop), crop residue management (0% to 100% of crop residues coverage), number of sugarcane cycles, and management level (low, medium and high).

In this study, we assumed four cover management scenarios to assign soil loss based on the yield average of the five sugarcane cycles and the ratio of 120 kg of dry matter straw per ton of fresh sugarcane stalk [50]. The scenarios are classified in: (i) no straw coverage rate (0 Mg^{-1}), (ii) 50% coverage (3.5 Mg^{-1}), (iii) 75% coverage (5.25 Mg^{-1}), and (iv) 100% coverage (7 Mg^{-1}).

SRL is calculated for a given condition using five subfactors and has to be calculated for different periods, as [9] recommended. Each subfactor contains cropping and management variables that affect soil erosion. PLU (Prior-Land Use) expresses the influence on soil erosion of subsurface residual effects from previous crops and the effect of previous crop management practices on soil consolidation. CC (Canopy Cover) indicates the effectiveness of vegetative canopy in reducing the energy of the rainfall striking the soil surface. SC (Surface Cover) affects erosion by reducing the transport capacity of runoff water by causing deposition in ponded areas and decreasing the surface area susceptible to raindrop impact. SR (Surface Roughness) is a function of the surface's random roughness. SM (Soil Moisture) influences infiltration, runoff, and soil erosion [9]. Here, soil moisture reflects the soil field capacity, value 1, due to their intensive condition under the erosive process.

$$\mathrm{SLR} = \mathrm{PLU} * \mathrm{CC} * \mathrm{SC} * \mathrm{SR} * \mathrm{SM} \tag{9}$$

$$Fator\ C = \sum_{i=1}^{12} \frac{SLR_i EI_i}{EI_{anual}} \tag{10}$$

EI_i is the rainfall erosivity for the month i (MJ mm^{-1} h^{-1} y^{-1}), and EI_{anual} is the annual rainfall erosivity (MJ mm^{-1} h^{-1} yr^{-1}).

2.4. Soil Loss Tolerance

Various methods to assess soil loss tolerance have been recommended by soil scientists worldwide; each approach has its assumptions, advantages, and limitations [51]. Land cover and carbon stocks are the principal indicators to estimate land degradation because they can change rapidly [52]. Here, the spatial modeling of soil loss tolerance was estimated based on [53] (Equation (13)), which considers the soil bulk density method obtained in [54] (Equations (11) and (12)) that depends on SOM and soil drained capacity. The soil class map of the agroindustry determined the soil drained capacity. The SOM map was estimated by the satellite bare soil surface methodology (Item 2.3.2). A soil depth of 0 to 0.30 m, and the temporal constant founded on the concept that forming 1000 mm of soil required 1000 years [55], were incorporated in the calculations to obtain T.

$$BD = 1.52 - 0.06 * SOM \text{ (well drained)} \quad (11)$$

$$BD = 1.53 - 0.5 * SOM \text{ (imperfectly drained)} \quad (12)$$

where BD is soil bulk density (g cm^{-3}), and SOM is organic matter (%)

$$T = \left(\frac{H \times BD}{1000}\right) * 10000 \quad (13)$$

BD is soil bulk density (kg m^{-3}). SOM is soil organic matter (g kg^{-1}). T is soil loss tolerance (Mg ha^{-1} yr^{-1}), H is soil depth (m), and 1000 is the temporal constant founded on the concept that forming 1000 mm of soil required 1000 years [53]; a 10,000 factor was applied to transform the data from Mg m^{-2} to Mg ha^{-1}.

3. Results

3.1. Soil Degradation Spatial Analyses Estimated by RUSLE

3.1.1. Rainfall Erosivity Factor

The spatial data average rainfall erosivity calculated represents 6078.00 MJ mm^{-1} ha^{-1} yr^{-1} (Figure 3), which according to [34,54] indicates strong erosivity, 300% higher than the global average [5].

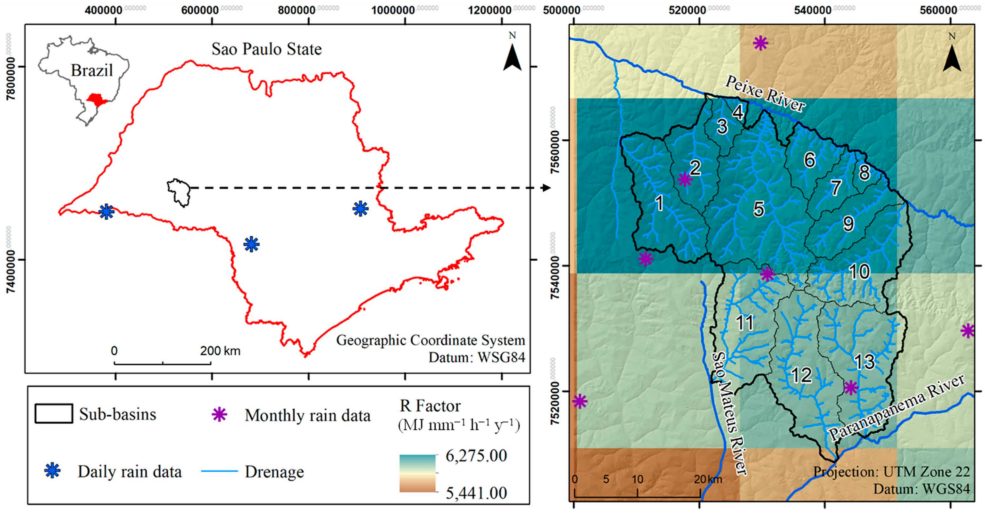

Figure 3. The sub-basins' geographic location with the distribution of daily rain data gauges in Sao Paulo State, Brazil and the monthly rain data gauges on the rainfall erosivity (R-Factor) map.

We calculated the R-Factor using TRMM data between 2008 and 2017 and the erosivity equations obtained by the daily rain data as a function of the Modified Fournier Index (MFI) (Figure 3). We compared our estimated R-Factor to that calculated from the monthly rain data gauges covering the sub-basins. In the southeastern part of Brazil, the rainy period

marks are that warm temperatures start in September and end in May (Figure 4a). The relation has an R^2 = 0.90, demonstrating a good correspondence between the values with a close 1:1 relationship (Figure 4b).

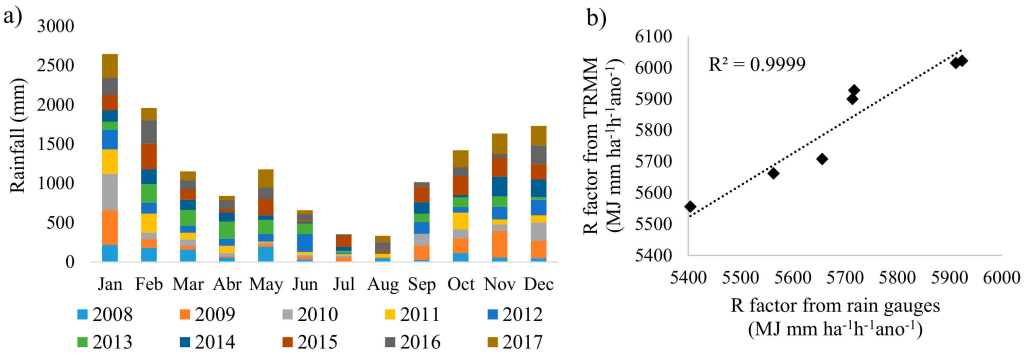

Figure 4. (**a**) Annual rainfall distribution from 2008 to 2017 from a station located in the study site, (**b**) R-Factor obtained from the Tropical Rainfall Measuring Mission (TRMM) compared to that obtained from the monthly rain gauges data.

3.1.2. Soil Erodibility Factor Obtained from the Digital Soil Attributes Mapping

The summary statistics of the soil property in Table 4 show soil attributes physical and organic matter variability at 0 to 0.30 m depth (Table 4). The low amount of clay and SOM content and high sand content ranging from 73% to 92% demonstrate soil erosion-prone features and the low natural fertility in the soil.

Table 4. Soil attributes values obtained by laboratory analyses.

	Minimum	Maximum	Mean	SD [1]	CV [2]
Sand (%)	73.00	92.10	83.27	4.11	16.87
Coarse Sand (%)	42.00	72.70	58.65	7.48	56.01
Fine Sand (%)	13.10	40.50	24.54	5.33	28.38
Silt (%)	1.20	3.80	2.07	0.56	0.32
Clay (%)	6.70	23.20	14.74	3.64	13.25
SOM [3] (%)	0.70	2.10	1.19	0.19	0.04

[1] Standard deviation; [2] Coefficient of variation; [3] Soil organic matter.

The geology map [25] showed that the sandy–mudstone lithology of the Rio do Peixe Valley's formation is predominant along with the site where the relief is flat featuring Ferralsol (LV, LA, LVA) to gentle undulations characterizing Lixisol (PV, PA, PVA) (Figure 5 and Table 5) [55]. By approaching the rolling uplands, the sandstone from the Marilia formation arises. Basic intrusive diabase rocks occur between the sand–mudstone of the Serra Geral formation neighboring the site, which provides the reddish color to the soil types and clay accumulation in the Lixisol subsurface (Figure 5). Ferralsols, Lixisol, and Gleysols represent 40%, 58%, and 2% of the land, respectively.

Soil permeability was established based on soil type, color and texture (Figure 5 and Table 5). The permeability decreases as color changes from reddish to yellowish and from sandy to clay texture. We classified the soil classes, in dry conditions, from the agroindustry map and the regional map [56] at the suborder level according to the Brazilian Soil Classification System (SiBCS) [57] and the corresponding classes of the World Reference Base [58].

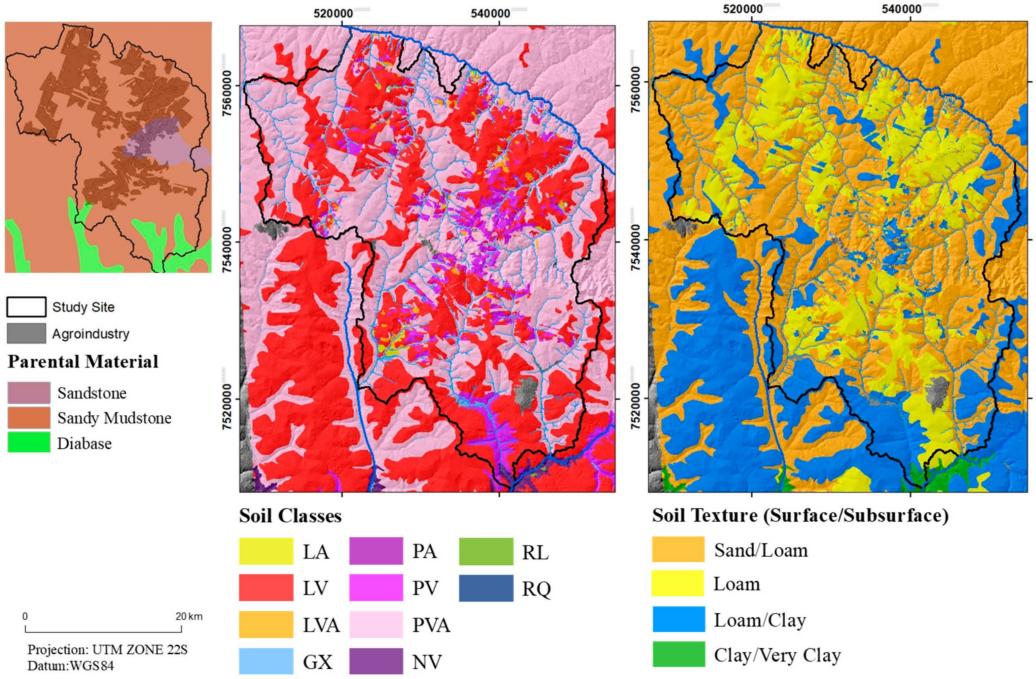

Figure 5. Maps of: (**left**) Lithology, (**middle**) Soil classes, (**right**) Topsoil class texture. Geological map, 1:100.000 scale [59].

Table 5. Permeability according to soil class type, color and texture [55].

SiBCS [1]	WRB [2]	Color	Texture	Permeability
Gleissolo Háplico (GX)	Gleysol			Very Slow
Latossolo Amarelo (LA)	Ferralsol	Yellow	Loam	Moderate
Latossolo Vermelho (LV)	Ferralsol	Red	Loam	Moderate to Fast
Latossolo Vermelho (LV)	Ferralsol	Red	Clay	Moderate
Latossolo Vermelho-Amarelo (LVA)	Ferralsol	Red -Yellow	Loam	Moderate to Fast
Latossolo Vermelho-Amarelo (LVA)	Ferralsol	Red -Yellow	Clay	Moderate
Nitossolo Vermelho (NV)	Nitosol	Red	Clay	Moderate to Fast
Argissolo Amarelo (PA)	Lixisol	Yellow	Sand/Loam	Slow to Moderate
Argissolo Amarelo (PA)	Lixisol	Yellow	Loam/Clay	Slow
Argissolo Vermelho (PV)	Lixisol	Red	Sand/Loam	Slow to Moderate
Argissolo Vermelho (PV)	Lixisol	Red	Loam/Clay	Slow
Argissolo Vermelho-Amarelo (PVA)	Lixisol	Red-Yellow	Sand/Loam	Slow to Moderate
Argissolo Vermelho-Amarelo (PVA)	Lixisol	Red-Yellow	Loam/Clay	Slow
Neossolo Litólico (RL)	Leptsol		Clay	Slow
Neossolo Quartzarênico (RQ)	Arenosol		Sand/Loam	Fast

[1] Brazilian Soil Classification System [57]. [2] World Reference Base [60].

The multi-temporal satellite bare soil resulted in 35 years of Landsat data from 1984 to 2019 (Figure 6a). The synthesis of all images composes a final image of bare soil, covering 72% of the cropland surface (Figure 6b). The soil surface corresponds to the agricultural inventory data, in which there is a specific time window to monitor soil surface satellite imaging due to the conventional crop management tillage adopted. The remaining sites correspond to forest or grass assigned as NA values for modeling.

The spatial–spectral patterns are related to the soil mineralogy, granulometry and organic matter content identified throughout the satellite image's color and the spectral data (Figure 6c). Bright colors indicate low soil organic carbon content and higher quartz proportions [40]. The shape and intensity of the spectral profile discriminate sandy soil as it increases from the higher reflectance and the ascending shape of the wavelength from Band 1 to Band 5 [39].

The spectral signatures of the surface reflectance provided from the site-specific soil samples validate the bare soil composite image's reliability and quality. Meanwhile, the

validation prediction of clay, fine sand, silt, and organic matter maps corresponds to R^2 of 0.67, 0.59, 0.68 and 0.55 and RMSE (g kg^{-1}) of 25.8, 48.3, 4.38, and 1.99, respectively, which indicates good agreement and low error between the observed and the predicted dataset.

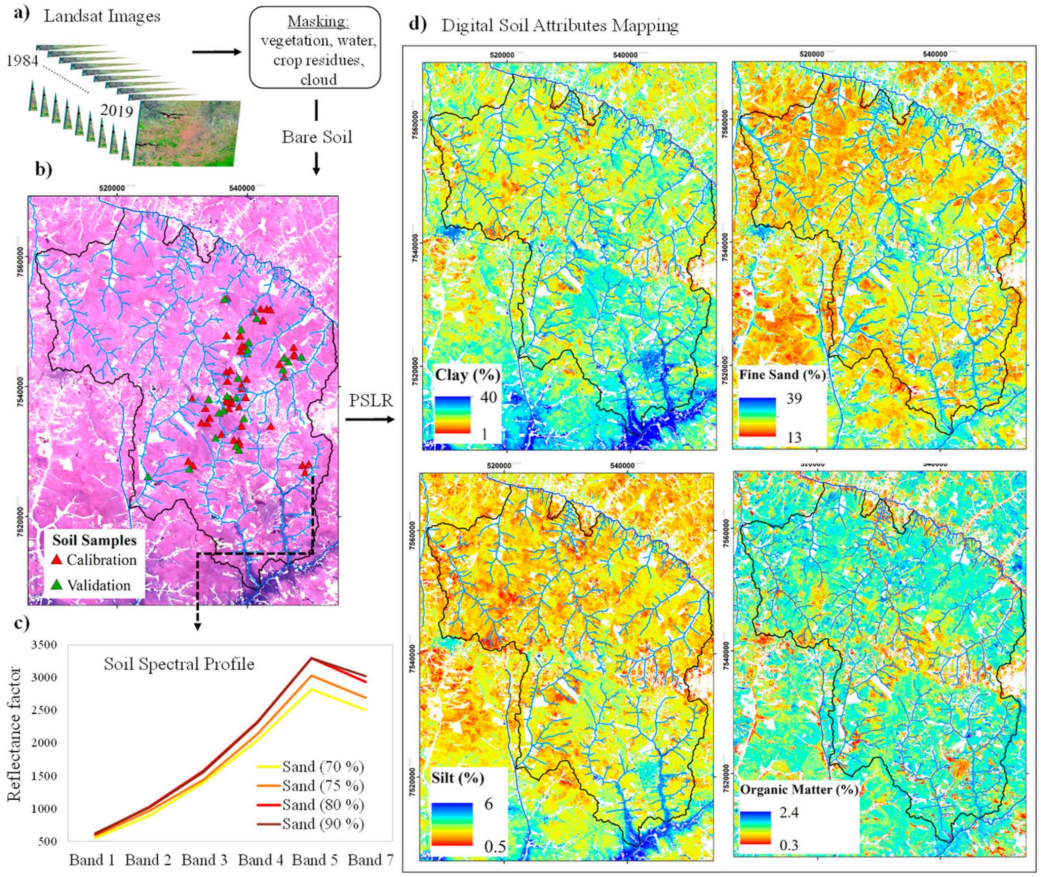

Figure 6. (**a**) Multi-temporal satellite images masks using NDVI and Mid-Infrared, (**b**) Soil Synthetic Image has shown the agricultural land in false color (RGB 543) of the Landsat data with the soil samples sites location used for the soil map attributes prediction by Partial Square Least Regression, (**c**) Soil spectral profile average from the soil samples, (**d**) Soil attributes map (clay, fine sand, silt, and organic matter) used to derive the erodibility factor map. Soil texture analyzes resulted in the following classes: Sand, Coarse Sand, Fine Sand, Silt and Clay. Note that only Clay, Fine Sand and Silt maps were generated to calculate erodibility, so the final percentage value will not be 100%. This would require all maps of all textural classes to reach 100%.

The spatial distribution of K-Factor values increases where PVA and PV occur in rolling uplands, as observed in the sub-basin 10 (Figure 7). In these sites, the sand–loamy textures soil particles are easily detached and transported by overland flow. The mean K-Factor value for the agricultural study site corresponds to 0.019 tons h MJ^{-1} mm^{-1}. Predicted versus measures K-Factor values present satisfactory performance with an R^2 of ~0.78 (Figure 8).

3.1.3. The Topographic Parameters and Control Practice

The LS-Factor derived from flow accumulation, flow direction, and slope using a Digital Elevation Model (DEM) performed by GIS incorporates surface runoff into soil erosion (Figure 9). The L-Factor stretches the impact of slope length while the S-Factor delivers the effect of slope steepness. The DEM captured the topography changes with precision and estimated soil erosion with accuracy. Ref. [45] demonstrated that the LS-Factor model is suitable for landscape-scale soil erosion modeling.

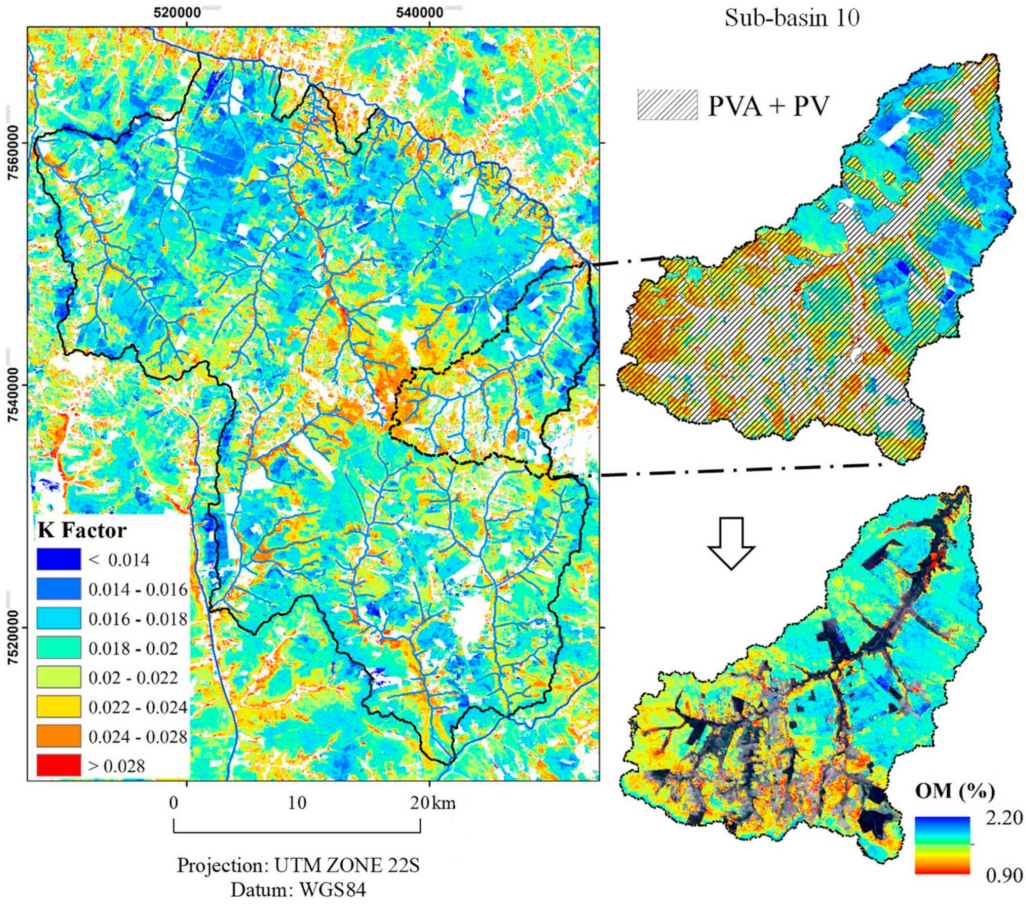

Figure 7. Soil K-Factor derived from satellite base estimation contrasting organic matter values at sub-basin 10.

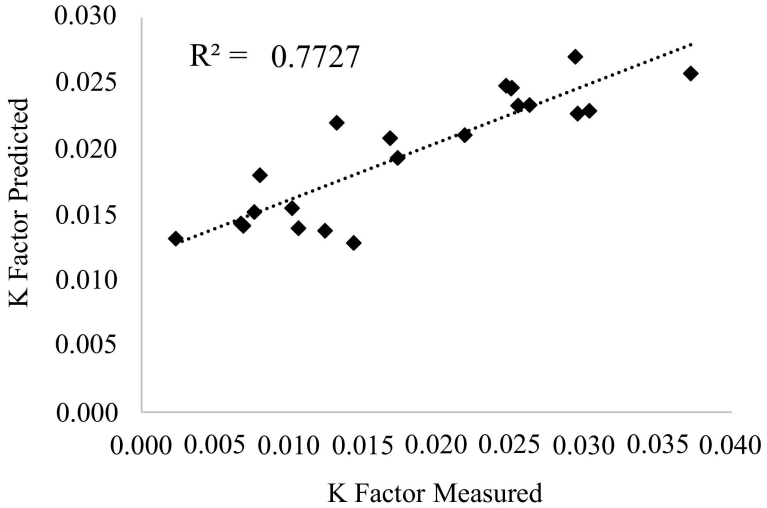

Figure 8. Comparison between the K-Factor satellite-based predicted and K-Factor measured by the soil samples analysis.

The LS-Factor's topographic spatial pattern presents an average value of 0.58, with a range of 0.03 in lowland to 82 in the uplands (Figure 8). The coefficient of variation (CV) of 0.53 indicates low heterogeneity; the LS-Factor value under 1.5 was estimated in 93% of the area.

The P-Factor map depended on the slope derived from DEM and contouring as specific support management (Figure 8). The P-Factor result presents low variation; 88% of the area has represented a value from 0.5 to 0.6 with an average of 0.59.

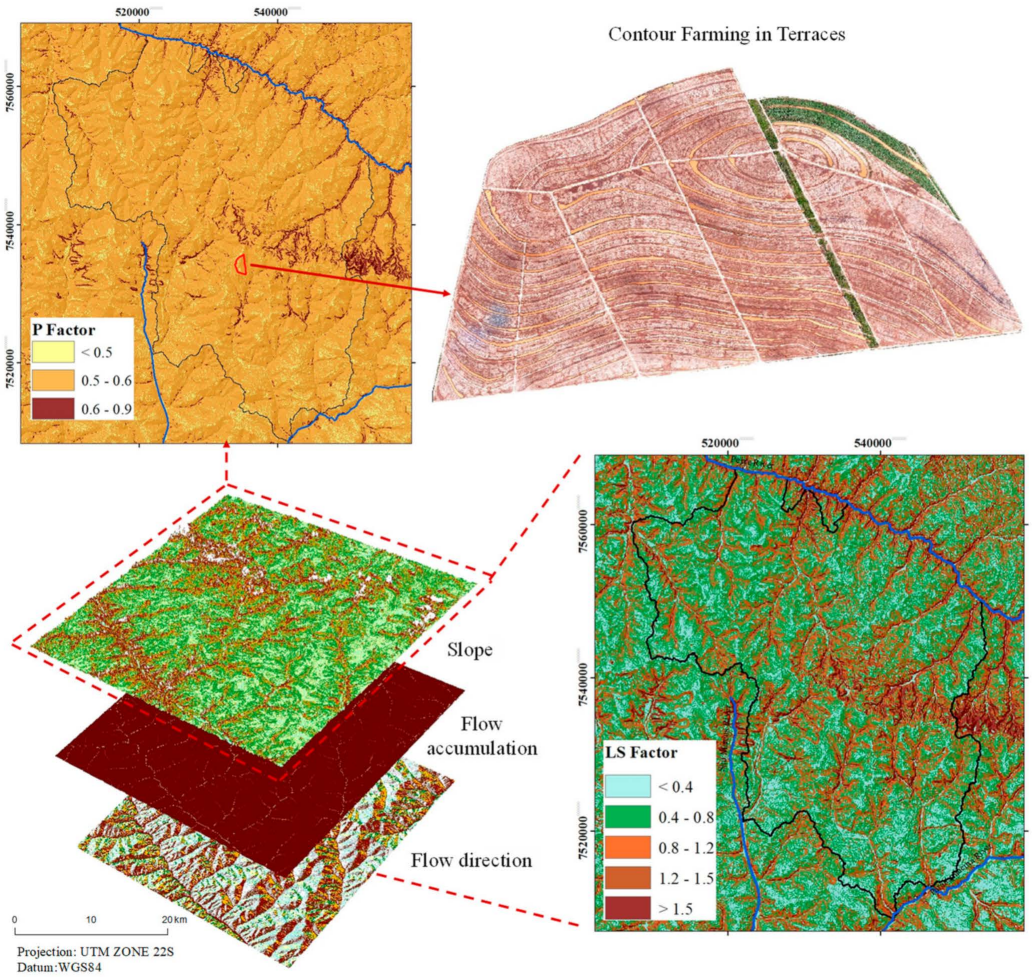

Figure 9. LS-Factor derived from the SRTM variables (slope, flow accumulation and flow direction) and P-Factor derived from slope and contour framing a support conservation practice.

3.1.4. Cover Management Factor

The spatial C-Factor of crop residue management for the scenarios expresses the land use management applied from 2013 to 2017 (Figure 10). It generated 98 combinations of sugarcane management in the cropland plots. We can observe in sub-basin 7 the cropland plots contrasting two tillage combinations. The sugarcane cycles range from one to nine in the unit plots; the mean is five crop cycles (Figure 11). During the sugarcane crop cycle, plant cane had higher production and yield decay over the next years (Figure 11b). We can observe that about 80% of the area is productive during the year, while the remaining area is under replanting (Figure 11a).

During the sugarcane replanting period, the crop residues are incorporated into the soil by tillage operations, and the soil is exposed, characterizing the prior land use subfactor as bare soil for all the cropland plots. The average C-Factor values from the cropland plots for 0%, 50%, 75%, and 100% coverage are 0.12, 0.0975, 0.0921 and 0.0884, respectively. We applied this C-Factor value for the entire sub-basins dimension.

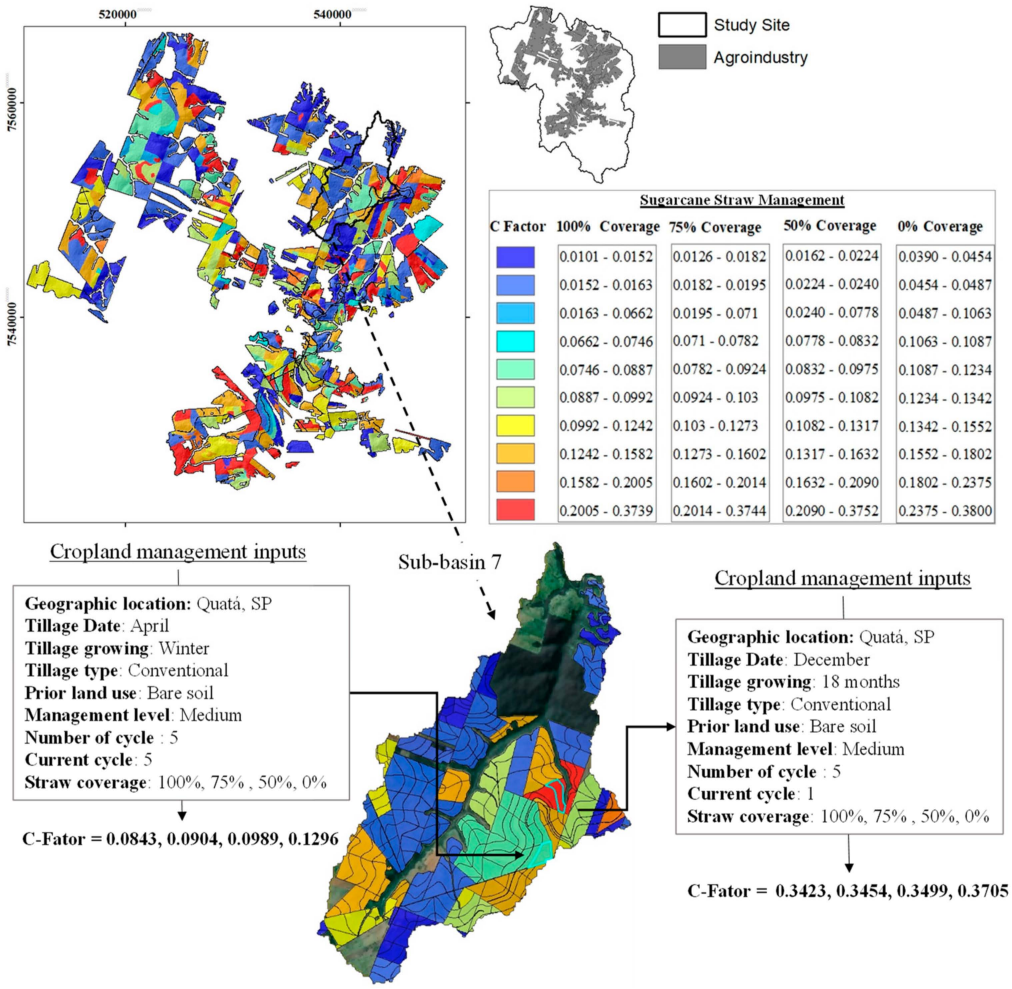

Figure 10. C-Factor of the agroindustry under 100% sugarcane straw coverage, 50% coverage, 75% coverage, and no coverage, and the sub-basin 7 representing two cover management input data in each arable cropland plot.

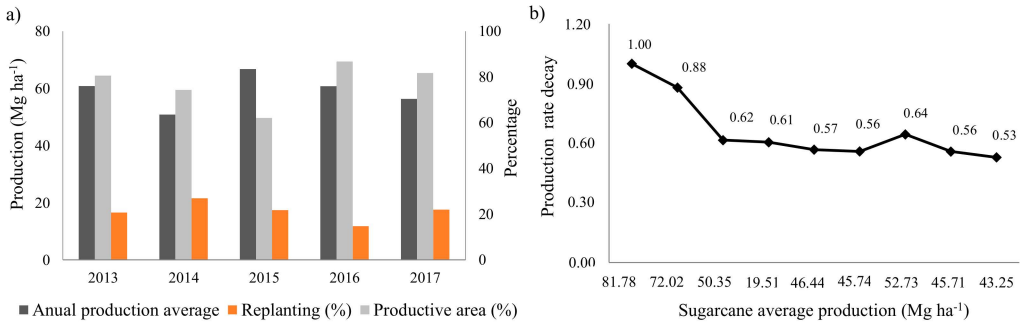

Figure 11. (**a**) Yield production areas from 2013 to 2017 with an average annual production considering all sugarcane cycles and the replanting areas. (**b**) The average yield in nine sugarcane crop cycle with production rate decay.

3.2. Soil Loss in Agricultural Regions

The soil loss rates from high-resolution spatially distributed modeling (30 × 30 m cell size) were estimated by integrating the erosivity, erodibility, topography, conservative practices, and cover management data. Our results showed that soil erosion dynamics under different straw coverage rates (Figure 12) decreases soil loss rates by 22%, 26% and 28% in all sub-basins as the amount of straw coverage increases to 50%, 75%, and 100%, respectively (Table 6).

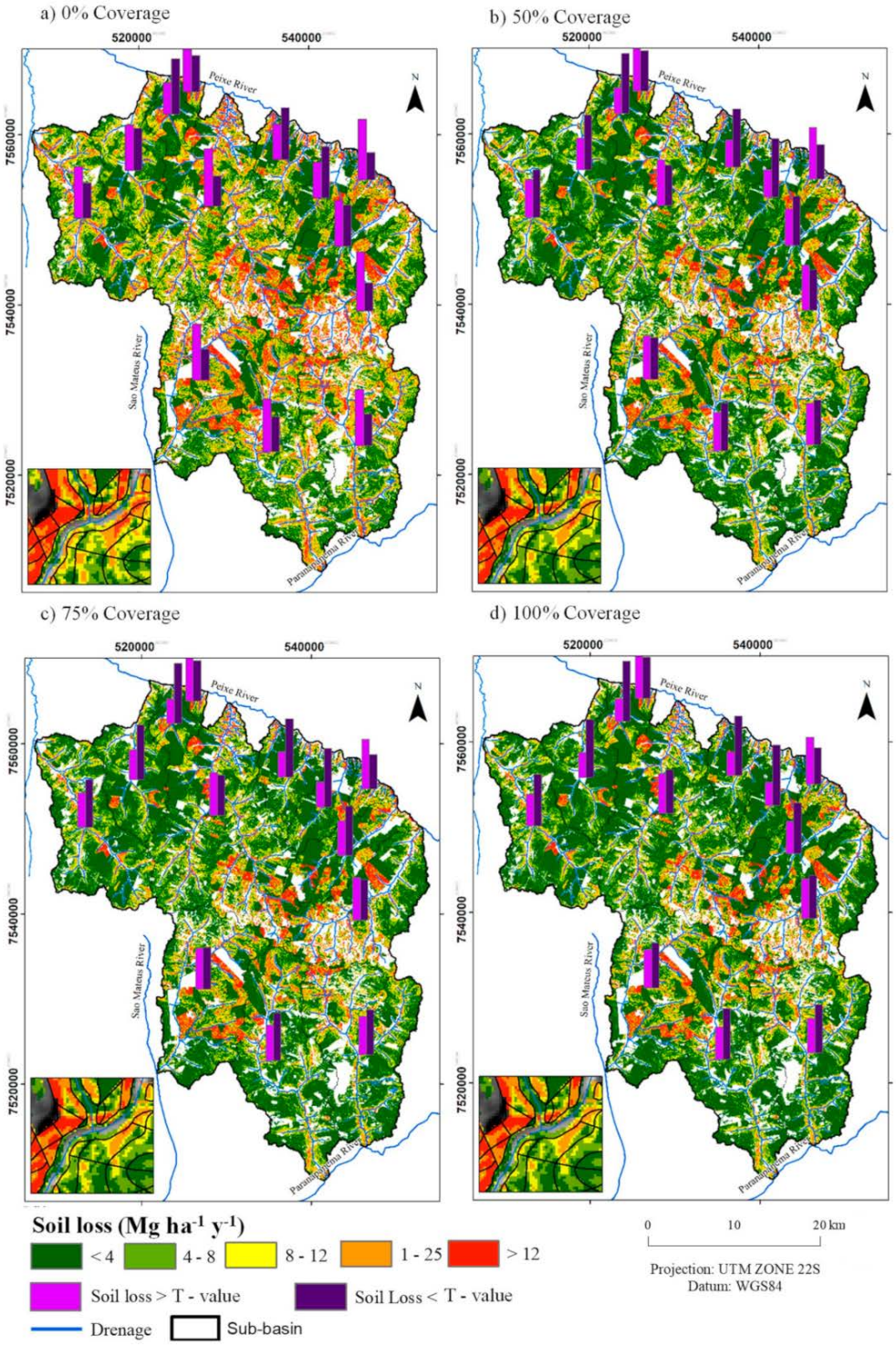

Figure 12. Soil loss obtained by the RUSLE model and the percentage of the basin with greater and lesser soil loss than the tolerance (T-value) with (**a**) 0% straw coverage rate, (**b**) 50% straw coverage, (**c**) 75% straw coverage, and (**d**) 100% straw coverage.

The average bulk density of 1.69 Mg m^{-3} derived soil loss tolerance (T-value); the T-value presents an area-specific average of 4.3 Mg ha^{-1}. Our data demonstrate that the annual average soil erosion exceeds the T-value threshold in 12 of the 13 sub-basins under no cover of straw (Table 6). Sub-basins 3, 6, and 7 show soil loss per percentage of the land lower than the T-value (Figure 12a).

Table 6. Average soil erosion and total soil loss per sub-basin.

Sub-Basin	Average Soil Erosion (Mg ha^{-1} yr^{-1})				Total Soil Loss (Mg × 10^3 yr^{-1})			
	0%	50%	75%	100%	0%	50%	75%	100%
1	5.74	4.35	4.10	3.93	832.09	631.024	494.67	569.71
2	4.83	3.73	3.59	3.39	432.27	333.741	321.65	303.37
3	4.19	3.31	3.14	3.02	125.86	99.25	94.10	90.48
4	7.53	6.39	6.18	6.04	65.65	55.69	53.90	52.65
5	6.11	4.82	4.58	4.41	1645.55	1297.30	1232.67	1188.52
6	4.59	3.33	3.09	2.93	269.72	195.55	181.72	172.24
7	4.89	3.75	3.52	3.35	206.67	158.49	148.60	141.68
8	7.30	5.70	5.38	5.16	103.54	80.87	76.35	73.28
9	6.52	5.10	4.79	4.57	535.56	419.43	393.70	375.45
10	7.62	5.84	5.50	5.26	942.35	722.981	680.03	650.71
11	6.97	5.64	5.37	5.18	1093.39	883.75	841.35	811.81
12	5.86	4.59	4.35	4.18	1050.64	822.95	780.04	750.33
13	6.38	4.92	4.65	4.46	1102.66	850.13	803.35	771.01
Total area	6.04	4.73	4.48	4.30	8406.01	6551.20	6202.47	5951.31

The most intensively eroded region were identified in sub-basins 4, 8, 9, 10, 11, 13 with an annual average soil erosion higher than the T-values in sites 100% covered with straw (Table 6). Sub-basin 4 presented the lowest values of total soil loss (52.65 Mg × 10^3 yr^{-1}) (Table 4), which was due to the smaller size of the sub-basin compared to the others. The average soil loss scenario of 100% straw coverage is equivalent to the T-value (Table 6), indicating that all the amount of straw is necessary to balance soil loss tolerance from the perspective of soil erosion. Thus, it is equivalent to 7 Mg^{-1} of straw according to the sugarcane yield data documented (Figure 11). However, this amount of straw has not been satisfactory to protect the soil against erosion in 40% of the agricultural land, which was classified with a higher potential of soil erosion estimated at ~6000 Mg 103 y^{-1} (Figure 12a, Table 6). We estimated an overall increase in soil erosion amount of 4%, 10%, and 41% under 75%, 50% and no coverage, respectively, which was driven by the possibility of spatial removal.

4. Discussion

The soil is vulnerable to erosion by nature according to a slow constructive process of fertile soils caused by geology, topography and climate factors. In contrast, anthropogenic land-use changes and unsustainable land management in agriculture can accelerate land degradation [4].

In this paper, we assessed a multi-temporal soil erosion pattern driven by water in sugarcane fields using the RUSLE model at 30 m resolution. We used remote sensing data and GIS techniques to extract R-, K-, and LS-Factors and an exhaustive set of C-Factors, an accurate DEM to compute LS- and P-Factors, and an innovative digital soil mapping method to calculate the K-Factor. Thus, the variability demonstrated by this method has a considerable potential to identify hotspots and concern areas for both uses in the cropland plots scale and the whole area for conservation planning (Figure 12).

Rainfall intensity emphasizes the region's climatic vulnerability, resulting in high values of erosivity factor (Figures 3 and 4), which is a critical climatic driver of soil erosion. According to [31], erosivity correlates with total rainstorm energy to the storm's maximum 30 min of rainfall intensity. The spatial variability of erosion power of rainfall tends to increase or decrease in various combinations driven to the degree of global warming caused by climate change [61], which impacts directly on land degradation, resulting in increasing temperatures, changing rainfall patterns, and intensification of rainfall [1].

Individual powerful rainstorms of a short period can remove topsoil during a rainstorm event, initiating a gully and mudslide, as revealed in Figure 1. Damages caused by heavy rainfall events have a century-scale nutrient depletion, soil particle loss, and

high-water treatment costs. The 3-hourly TRMM data provided a good indicator of high-intensity rainfall events (more than 30 mm), which were typically captured at the beginning of the rainy season [62].

Hydrological changes affect soil fertility due to topsoil layer removal, water availability, and the vulnerability of smallholder and subsistence agriculture [63]. Each soil type has properties that have different resistance to the raindrop and runoff. High rainfall erosivity increases soil loss rates that deplete the soil structure (breakdown aggregates) and accelerate the decomposition of the organic carbon matter by a microbial process [4]. Controversially, a decrease in rainfall erosivity may enforce agribusiness development [64] and smallholders, especially in regions with crop irrigation liability. Meanwhile, a decrease in rainfall erosivity in the southeast region of Brazil may suggest a favorable scenario for the continued sugarcane expansion [64] since sugarcane does not need irrigation [65].

The projection of climate change in rainfall erosivity is essential, but at this stage, developing strategies to adapt to these changes is the key to reduce vulnerabilities and improve resilience; e.g., public policies that focus on soil and water conservation such as sustainable agriculture and conservation practices must be encouraged, ensuring food security and energy.

Our digital soil attributes maps obtained extracted from satellite data are instruments for sustainable land use (Figure 6). Previous studies based on Landsat data have also derived reliable soil proprieties maps demonstrating the substantial potential of these products for the land management applications [66–69]. We identified that sites with moderate soil loss are mostly homogeneous with topsoil texture that varies from loam to sandy. The loam texture sites demonstrate the occurrence of Ferralsols (Figure 5) in the flat position of the landscape. On the other hand, high soil loss occurs mostly in Lixisol (Figure 5) that is over smooth to gently undulating relief with the textural gradient of sandy/loamy at the surface and loamy/clayey in subsurface layers (Figure 6), featuring the highest values of LS-Factor (Figure 9). We confirmed [70] assumption that an increase in the textural gradient leads to a decrease in soil loss tolerance and an increase in soil K-Factor (Figure 7).

SYSI data can capture the agricultural land-use change. Here, we could enlighten two time periods to investigate land-use change using SYSI: (1) from 1984 to 2009, the period with land changes from forestation to sugarcane under harvest burning system adoption; (2) after 2009, with the establishment of the current machine harvest system characterized by the remarkable effect of soil conservation agriculture provided by straw on topsoil. On the other hand, straw removal practices may threaten sugarcane yield, compromising bioenergy production [71]. The nutrient addition in soil in the first period, associated with straw removal of the second period plus the climate change impacts related to land use cover, may be responsible for soil organic matter depletion [16,71]. Our investigations reveal that the high erodibility values in sub-basin 10 correspond to Lixisols, which are associated with the low organic matter content (Figure 7). Lixisols when exposed due to changes in land use and/or soil management lead to erosion processes. These soils have a more clayey B horizon, which reduces water infiltration, favoring surface runoff and, consequently, erosion.

Strategies for soil conservation as cover management are the main component to control soil erosion runoff potential, maintain soil structure and conserve soil organic carbon with low cost [72]. Crop residue retained in the field delivers maintenance to the soil quality; it affects sugarcane yields in all soil types in different magnitudes. Straw can help maintain soil moisture and mitigate water deficit, which stimulates the microclimate by regulating the thermal amplitude and improving the soil biota [73,74]. The yield annual average, inferior to the national average yield of 76 Mg ha^{-1} [75] (Figure 11a) aggregated with soil compaction, reveals low soil fertility. Field observations and the literature indicated high soil compaction in this region, particularly if straw has been removed [17], which resulted in low soil permeability capacity.

Ferralsol is very well-developed, deep and unsaturated, and it is characterized as having fast permeability. However, this soil was classified as moderate to fast or moderate. We also observed that permeability decreases as the color changes from reddish to yellowish and sandy to clay texture (Table 5). Whereas, as permeability decreases, Lixisol is more vulnerable to topsoil loss, which is well-developed with a textural gradient in the subsurface featuring erosion-prone soils [76]. These attributes result in low yielding potential and straw production. It explains the inefficiency of 100% straw coverage capacity of holding gross erosion and preventing soil degradation in many sub-basins, especially in sub-basins 4 and 8 that presented the soil erosion hot spots (Figure 12d and Table 6) even under a low heterogeneity topography (Figure 9).

Our C-Factor results demonstrate that the number of sugarcane cycles and the planting season are the SRL that have the most significant impact on the management cover, which is consistent with [49]. The sugarcane cycle can influence the crop residue maintenance in the erosion process by surface cover, canopy cover, and tillage effectiveness in the yielding. While the planting season is affected by the climate, the soil is affected by the following conditions: (i) during replanting, when the soil is entirely uncovered; (ii) at the beginning of the sugarcane ratoon, the previous cycle removed the straw, and the sugarcane canopy cover is not entirely close; (iii) the low number of sugarcane cycles (less than five due to the low yield and coverage potential; and (iv) tillage management operations during the rainy season.

Alternative management strategies on-site for more sustainable sugarcane production are required to compensate for the adverse erosion effects on soil, water, and biotic balance as vegetative barrier conservation practices [77]. Techniques to improve soil organic carbon and increase yield include reduce or no-tillage, crop rotation (minimum soil disturbance) [16], legume cover crop [78], organic fertilizer, filter cake, ashes, biochar, and others. Reduce tillage and no-tillage system concepts were implemented in this century. A reduced tillage system associated with a part of the straw cover in the soil could enhance the soil organic carbon stock, sustain sugarcane yield over the crop cycle, and allow part of the straw to be used for bioenergy [16]. Each agricultural system affects short-term soil CO_2 emissions. Undisturbed soil keeps higher soil moisture than conventional tillage; moisture is a control temporal variability factor of CO_2 emission. The adoption of no-tillage in sugarcane areas would prevent 30% of soil CO_2 emission in tropical soils compared with conventional tillage.

The erosion cost could be reduced by 81.2% adopting no-tillage, while the production costs increased only by 0.47 for the soybean crop [79]. Another study observed the same crop and an erosion cost reduction from the different management systems, including no-tillage, reduced tillage and conventional tillage of USD 15, 16, and 25 ha^{-1} yr^{-1}, respectively [80]. Soil erosion assessment is essential from an economic perspective since it degrades soils on-site, producing loss of fertility, and reduces water storage capacity, compromising yield, which over the long term may depreciate land value [81,82]. The hydrographic basins unit is vital to assess the cost of soil loss due to the off-site impacts of land degradation. Soil erosion effects in the surrounding areas can be severe to the freshwater systems causing sedimentation and eutrophication, enhancing urban areas flooding, and impacting the marine ecosystem.

The results reported herein indicate that conservation-effective measures to address on-site erosion are essential to reduce or reverse soil degradation and minimize the climate change impacts from off-site erosion. Furthermore, the obligation of soil conservation practices may help to internalize the costs of the land user. Fertile soil is a limited and non-renewable natural resource, and soil degradation impacts the world from many aspects, e.g., socio-economic, social, political, and cultural for current and future generations.

5. Conclusions

The method to estimate soil loss indicated soil degradation-prone areas that require sustainable land management. The bare soil surface image obtained from multi-temporal

satellite images covering 100% of the agricultural land use is equivalent to 72% of the study site. The image's spectral patterns presented an accurate spectral quality that permits capturing the soil interactions, featuring sandy soil and low organic matter content properties. Our spatiotemporal erodibility factor reveals the correlation of soil organic matter depletion with high erodibility values in Lixisol, which resulted in low soil loss tolerance.

The bare soil surface technique indicates that intensive farming caused high soil exposure rates in the last three decades. Erosion intensification has contributed to land degradation for at least 20 years from the beginning of the multi-temporal series until 2010, when bare soil frequency decreased due to the gradual change to agricultural conservation systems established in the sugarcane fields. Our result indicates vulnerable areas to hold gross erosion in locations with 100% crop residue coverage. This susceptible area is a combination of natural erosion-prone areas with low effectiveness of the tillage practices and the number of cycles (inferior to five) that result in low sugarcane straw yield, which is easily and quickly decomposed by the microbial process. In addition, we suggest further studies using SYSI to deepen soil erosion research.

Furthermore, the strong rainfall erosivity of the region reinforces soil erosion by water, especially in the planting season. Public policies that focus on soil and water conservation to ensure food and energy security are strategies to reduce the vulnerabilities and improve the resilience of the environment to adapt to the increasing temperatures, the changing of the rainfall patterns, and the rainfall intensification driven by climate change. This technique provides multidisciplinary uses that extend beyond sustainable agriculture developments and land-use change monitoring as the costs to replace nutrients loss derived from soil erosion and carbon stock dynamics are the foundation for the emission levels analyses.

The high-resolution spatially distribution method provided can identify soil degradation-prone areas and the cropland expansion frequency. This information may guide farms and the policymakers for a better request of conservation practices according to site-specific management variation.

Author Contributions: B.C.G., P.S.G.M. and J.A.M.D. conceived the main idea; W.R.C. contributed to the methodology development; J.L.N.C. and L.C.B. organized the field experiments; The manuscript was written by B.C.G. and improved by D.C.d.M., L.C.B., H.B. and J.L.N.C.; The following authors performed the validation: E.I.F.-F., M.R.F., G.V.V., C.E.G.R.S., M.R.A. P.S.G.M., J.A.M.D. and J.L.N.C. were responsible for the acquisition of the financial support for the project leading to this publication. All authors have read and agreed to the published version of the manuscript.

Funding: This study was financed in part by the "Coordenação de Aperfeiçoamento de Pessoal de Nível Superior—Brasil" (CAPES)—Finance Code 001. This study was also supported by the Sugarcane Renewable Electricity project–SUCRE/PNUD (grant number BRA/10/G31), by the São Paulo Research Foundation (FAPESP) (grant No. 2014-22262-0, 2014-14965-0, 2015-01587-0, and 2017-03207-6), and by The Global Affairs Canada for the scholarship through the 2018 Emerging Leaders in the Americas Program (ELAP).

Data Availability Statement: Not applicable.

Acknowledgments: We are grateful to CAPES, FAPESP, Project-SUCRE, and Global Affairs Canada for providing the research grants. We would like to thank the LNBR technician group for all the support in the field and laboratory activities and Quatá Milll for providing the experimental sites and the logistical support during the fieldwork. We also are grateful to Dongmei Chen for the research development support at Queens University and the Geotechnologies in Soil Science group (GeoSS—website http://esalqgeocis.wixsite.com/english).

Conflicts of Interest: The authors declare no conflict of interest.

References

1. Olsson, L.; Barbosa, H.; Bhadwal, S.; Cowie, A.; Delusca, K.; Flores-Renteria, D.; Hermans, K.; Jobbagy, E.; Kurz, W.; Li, D. Land degradation: IPCC special report on climate change, desertification, land 5 degradation, sustainable land management, food security, and 6 greenhouse gas fluxes in terrestrial ecosystems. In *IPCC Special Report on Climate Change, Desertification, Land 5*

Degradation, Sustainable Land Management, Food Security, and 6 Greenhouse Gas Fluxes in Terrestrial Ecosystems; Intergovernmental Panel on Climate Change (IPCC): Geneva, Switzerland, 2019; p. 1.
2. Panagos, P.; Borrelli, P.; Robinson, D. FAO calls for actions to reduce global soil erosion. *Mitig. Adapt. Strateg. Glob. Chang.* **2020**, *25*, 789–790. [CrossRef]
3. Montgomery, D.R. *Dirt: The Erosion of Civilizations*; University of California Press: Oakland, CA, USA, 2012; ISBN 0520272900.
4. Lal, R. Soil erosion and the global carbon budget. *Environ. Int.* **2003**, *29*, 437–450. [CrossRef]
5. Borrelli, P.; Robinson, D.A.; Fleischer, L.R.; Lugato, E.; Ballabio, C.; Alewell, C.; Meusburger, K.; Modugno, S.; Schütt, B.; Ferro, V.; et al. An assessment of the global impact of 21st century land use change on soil erosion. *Nat. Commun.* **2017**, *8*, 2013. [CrossRef]
6. Lorenz, K.; Lal, R.; Ehlers, K. Soil organic carbon stock as an indicator for monitoring land and soil degradation in relation to United Nations' Sustainable Development Goals. *Land Degrad. Dev.* **2019**, *30*, 824–838. [CrossRef]
7. Montanarella, L.; Scholes, R.; Brainich, A. (Eds.) IPBES The IPBES assessment report on land degradation and restoration. In *Secretariat of the Intergovernmental Science-Policy Platform on Biodiversity and Ecosystem Services, Bonn, Germany*; Intergovernmental Science-Policy Platform on Biodiversity and Ecosystem Services: Bonn, Germany, 2018; pp. 1–744, ISBN 9783947851096.
8. Wischmeier, W.H.; Smith, D.D. *Predicting Rainfall Erosion Losses: A Guide to Conservation Planning*; USDA: Washington, DC, USA, 1978.
9. Renard, K.G.; Foster, G.R.; Weesies, G.A.; Mccool, D.K.; Yoder, D.C. *Predicting Soil Erosion by Water: A Guide to Conservation Planning with the Revised Universal Soil Loss Equation (RUSLE)*; U.S. Depar.: Washington, DC, USA, 1997; ISBN 0160489385.
10. Ostovari, Y.; Ghorbani-Dashtaki, S.; Bahrami, H.A.; Naderi, M.; Dematte, A.M. Soil loss prediction by an integrated system using RUSLE, GIS and remote sensing in semi-arid region. *Geoderma Reg.* **2017**, *11*, 28–36. [CrossRef]
11. Teng, H.; Viscarra Rossel, R.A.; Shi, Z.; Behrens, T.; Chappell, A.; Bui, E. Assimilating satellite imagery and visible-near infrared spectroscopy to model and map soil loss by water erosion in Australia. *Environ. Model. Softw.* **2016**, *77*, 156–167. [CrossRef]
12. Walter, A.; Galdos, M.V.; Scarpare, F.V.; Verde Leal, M.R.L.; Abel Seabra, J.E.; da Cunha, M.P.; Araujo Picoli, M.C.; de Oliveira, C.O.F. Brazilian sugarcane ethanol: Developments so far and challenges for the future. *Adv. Bioenergy Sustain. Chall.* **2016**, 373–394. [CrossRef]
13. de OR Medeiros, G.; Giarolla, A.; Sampaio, G.; Marinho, M.D.A. Estimates of annual soil loss rates in the state of São Paulo, Brazil. *Rev. Bras. De Ciência Do Solo* **2016**, *40*, 1–18. [CrossRef]
14. Carvalho, J.L.N.; Nogueirol, R.C.; Menandro, L.M.S.; Bordonal, R.D.O.; Clovis, D.B.; Cantarella, H.; Franco, H.C.J. Agronomic and environmental implications of sugarcane straw removal : A major review. *Bioenergy Res.* **2016**, *9*, 1–16. [CrossRef]
15. Cherubin, M.R.; Lisboa, I.P.; Silva, A.G.B.; Varanda, L.L.; Bordonal, R.O.; Carvalho, J.L.N.; Otto, R.; Pavinato, P.S.; Soltangheisi, A.; Cerri, C.E.P. Sugarcane Straw Removal: Implications to Soil Fertility and Fertilizer Demand in Brazil. *BioEnergy Res.* **2019**, *12*, 888–900. [CrossRef]
16. Tenelli, S.; de Oliveira Bordonal, R.; Barbosa, L.C.; Carvalho, J.L.N. Can reduced tillage sustain sugarcane yield and soil carbon if straw is removed? *BioEnergy Res.* **2019**, *12*, 764–777. [CrossRef]
17. Castioni, G.A.F.; Cherubin, M.R.; Bordonal, R.D.O.; Barbosa, L.C.; Menandro, L.M.S.; Carvalho, J.L.N. Straw Removal Affects Soil Physical Quality and Sugarcane Yield in Brazil. *BioEnergy Res.* **2019**, *12*, 789–800. [CrossRef]
18. Menandro, L.M.S.; de Moraes, L.O.; Borges, C.D.; Cherubin, M.R.; Castioni, G.A.; Carvalho, J.L.N. Soil Macrofauna Responses to Sugarcane Straw Removal for Bioenergy Production. *BioEnergy Res.* **2019**, *12*, 944–957. [CrossRef]
19. Martins-Filho, M.V.; Liccioti, T.T.; Pereira, G.T.; Marques Júnior, J.; Sanchez, R.B. Soil and Nutrients Losses of an Alfisol with Sugarcane Crop Residue. *Eng. Agric.* **2009**, *29*, 8–18.
20. Franco, H.C.J.; Pimenta, M.T.B.; Carvalho, J.L.N.; Magalhães, P.S.G.; Rossell, C.E.V.; Braunbeck, O.A.; Vitti, A.C.; Kolln, O.T.; Rossi Neto, J. Assessment of sugarcane trash for agronomic and energy purposes in Brazil. *Sci. Agric.* **2013**, *70*, 305–312. [CrossRef]
21. Carvalho, J.L.N.; Otto, R.; Junqueira Franco, H.C.; Ocheuze Trivelin, P.C. Input of sugarcane post-harvest residues into the soil. *Sci. Agric.* **2013**, *70*, 336–344. [CrossRef]
22. Jones, C.D.; Zhang, X.; Reddy, A.D.; Robertson, G.P.; Izaurralde, R.C. The greenhouse gas intensity and potential biofuel production capacity of maize stover harvest in the US Midwest. *GCB Bioenergy* **2017**, *9*, 1543–1554. [CrossRef]
23. Silva, A.G.B.; Lisboa, I.P.; Cherubin, M.R.; Cerri, C.E.P. How Much Sugarcane Straw is Needed for Covering the Soil? *BioEnergy Res.* **2019**, *12*, 858–864. [CrossRef]
24. de Oliveira Bordonal, R.; Menandro, L.M.S.; Barbosa, L.C.; Lal, R.; Milori, D.M.B.P.; Kolln, O.T.; Franco, H.C.J.; Carvalho, J.L.N. Sugarcane yield and soil carbon response to straw removal in south-central Brazil. *Geoderma* **2018**, *328*, 79–90. [CrossRef]
25. Perrotta, M.M.; Salvador, E.; Lopes, R.; D'Agostinho, L.; Peruffo, N.; Gomes, S.D.; Sachs, L.L.B.; Meira, V.T.; Garcia, M.G.M.; Lacerda Filho, J.V. *Mapa Geológico do Estado de São Paulo, Escala 1:750.000*; Programa levantamentos geológicos básicos do Brasil, CPRM: São Paulo, Brazil, 2005.
26. EMBRAPA. *Manual de Metodos de Analises*; Editorial Académica Española: Brasília, Brazil, 2017; ISBN 9788570357717.
27. IUSS Working Group WRB. *World Reference Base for Soil Resources 2014. International Soil Classification System for Naming Soils and Creating Legends for Soil Maps*; IUSS Working Group WRB: Rome, Italy, 2015.
28. Benavidez, R.; Jackson, B.; Maxwell, D.; Norton, K. A review of the (Revised) Universal Soil Loss Equation ((R) USLE): With a view to increasing its global applicability and improving soil loss estimates. *Hydrol. Earth Syst. Sci.* **2018**, *22*, 6059–6086. [CrossRef]

29. Borrelli, P.; Van Oost, K.; Meusburger, K.; Alewell, C.; Lugato, E.; Panagos, P. A step towards a holistic assessment of soil degradation in Europe: Coupling on-site erosion with sediment transfer and carbon fluxes. *Environ. Res.* **2018**, *161*, 291–298. [CrossRef] [PubMed]
30. U.S. Department of Agriculture, Agricultural Research Service and Soil Conservation Service. *Joint Conference on Slope-Practice*; USDA: Washington, DC, USA, 1956.
31. Vrieling, A.; Hoedjes, J.C.B.; van der Velde, M. Towards large-scale monitoring of soil erosion in Africa: Accounting for the dynamics of rainfall erosivity. *Glob. Planet. Chang.* **2014**, *115*, 33–43. [CrossRef]
32. Vrieling, A.; Sterk, G.; de Jong, S.M. Satellite-based estimation of rainfall erosivity for Africa. *J. Hydrol.* **2010**, *395*, 235–241. [CrossRef]
33. Huffman, G.J.; Bolvin, D.T.; Nelkin, E.J.; Wolff, D.B.; Adler, R.F.; Gu, G.; Hong, Y.; Bowman, K.P.; Stocker, E.F. The TRMM Multisatellite Precipitation Analysis (TMPA): Quasi-Global, Multiyear, Combined-Sensor Precipitation Estimates at Fine Scales. *J. Hydrometeorol.* **2007**, *8*, 38–55. [CrossRef]
34. Mello, C.R.; Viola, M.R.; Beskow, S.; Norton, L.D. Multivariate models for annual rainfall erosivity in Brazil. *Geoderma* **2013**, *202*, 88–102. [CrossRef]
35. Oliveira, P.T.S.; Wendland, E.; Nearing, M.A. Rainfall erosivity in Brazil: A review. *Catena* **2013**, *100*, 139–147. [CrossRef]
36. Colodro, G.; Carvalho, M.P.; Roque, C.G.; Prado, R.M. Rainfall erosivity: Its distribution and relationship with the nonrecording rain gauge precipitation at Teodoro Sampaio, São Paulo, Brazil. *Rev. Bras. De Ciênc. Do Solo* **2002**, *26*, 809–818. [CrossRef]
37. Lombardi Neto, F.; Moldenhauer, W.C. Erosividade da chuva: Sua distribuicao e relacao com as perdas de solo em Campinas (SP). *Bragantia* **1992**, *51*, 189–196. [CrossRef]
38. Roque, C.G.; Carvalho, M.P.; Prado, R.M. Fator erosividade da chuva de Piraju (SP): Distribuição, probabilidade de ocorrência, período de retorno e correlação com o coeficiente de chuva. *Rev. Bras. De Ciênc. Do Solo* **2001**, *25*, 147–156. [CrossRef]
39. Gallo, B.C.; Demattê, J.A.M.; Rizzo, R.; Safanelli, J.L.; Mendes, W.D.S.; Lepsch, I.F.; Sato, M.V.; Romero, D.J.; Lacerda, M.P.C. Multi-temporal satellite images on topsoil attribute quantification and the relationship with soil classes and geology. *Remote Sens.* **2018**, *10*, 1571. [CrossRef]
40. Demattê, J.A.M.; Safanelli, J.L.; Poppiel, R.R.; Rizzo, R.; Silvero, N.E.Q.; de Sousa Mendes, W.; Bonfatti, B.R.; Dotto, A.C.; Salazar, D.F.U.; de Oliveira Mello, F.A. Bare earth's Surface Spectra as a proxy for Soil Resource Monitoring. *Sci. Rep.* **2020**, *10*, 4461. [CrossRef]
41. Demattê, J.A.M.; Fongaro, C.T.; Rizzo, R.; Safanelli, J.L. Geospatial Soil Sensing System (GEOS3): A powerful data mining procedure to retrieve soil spectral reflectance from satellite images. *Remote Sens. Environ.* **2018**, *212*, 161–175. [CrossRef]
42. Safanelli, J.L.; Chabrillat, S.; Ben-dor, E.; Demattê, J.A.M. Multispectral Models from Bare Soil Composites for Mapping Topsoil Properties over Europe. *Remote Sens.* **2020**, *12*, 1369. [CrossRef]
43. Panagos, P.; Borrelli, P.; Meusburger, K. A New European Slope Length and Steepness Factor (LS-Factor) for Modeling Soil Erosion by Water. *Geosciences* **2015**, *5*, 117–126. [CrossRef]
44. Foster, G.R.; Meyer, L.D.; Onstad, C.A. A runoff erosivity factor and variable slope length exponents for soil loss estimates. *Trans. ASAE* **1977**, *20*, 683–687. [CrossRef]
45. Desmet, P.J.J.; Govers, G. A GIS procedure for automatically calculating the USLE LS factor on topographically complex landscape units. *J. Soil Water Conserv.* **1996**, *51*, 427–433.
46. Mccool, D.K.; Brown, L.C.; Foster, G.R.; Mutchler, C.K.; Meyer, L.D. Revised Slope Steepness Factor for the Universal Soil Loss Equation. *Trans. ASAE* **1987**, *30*, 1387–1396. [CrossRef]
47. Stevens, C.J.; Quinton, J.N.; Bailey, A.P.; Deasy, C.; Silgram, M.; Jackson, D.R. The effects of minimal tillage, contour cultivation and in-field vegetative barriers on soil erosion and phosphorus loss. *Soil Tillage Res.* **2009**, *106*, 145–151. [CrossRef]
48. Tanyaş, H.; Kolat, Ç.; Süzen, M.L. A new approach to estimate cover-management factor of RUSLE and validation of RUSLE model in the watershed of Kartalkaya Dam. *J. Hydrol.* **2015**, *528*, 584–598. [CrossRef]
49. Rocha, G.C. da Conservação do Solo e Cana-de-Açúcar: Aspectos Legais e Bibliométricos e Uma Ferramenta de Determinação do Fator C (RUSLE). Ph.D. Thesis, University of Sao Paulo, Sao Paulo, Brazil, 2017.
50. Menandro, L.M.S.; Cantarella, H.; Franco, H.C.J.; Kölln, O.T.; Pimenta, M.T.B.; Rabelo, S.C.; Carvalho, J.L.N.; Sanches, G.M. Comprehensive assessment of sugarcane straw: Implications for biomass and bioenergy production. *Biofuels Bioprod. Biorefin.* **2017**, *11*, 488–504. [CrossRef]
51. Yang, X.; Leys, J.; Gray, J.; Zhang, M. Hillslope erosion improvement targets: Towards sustainable land management across New South Wales, Australia. *Catena* **2022**, *211*, 105956. [CrossRef]
52. Chappell, A.; Webb, N.P.; Leys, J.F.; Waters, C.M.; Orgill, S.; Eyres, M.J. Minimising soil organic carbon erosion by wind is critical for land degradation neutrality. *Environ. Sci. Policy* **2019**, *93*, 43–52. [CrossRef]
53. Smith, R.M.; Stamey, W.L. Determining the range of tolerable erosion. *Soil Sci.* **1965**, *100*, 414–424. [CrossRef]
54. Foster, G.R.; McCool, D.K.; Renard, K.G.; Moldenhauer, W.C. Conversion of the universal soil loss equation to SI metric units. *J. Soil Water Conserv.* **1981**, *36*, 355–359.
55. Bertoni, J.; Lombardi Neto, F. *Conservação do Solo*, 10th ed.; Ícone editora: São Paulo, Brazil, 2017; ISBN 978-85-274-0980-3.
56. Rossi, M. *Mapa Pedológico do Estado de São Paulo: Revisado e Ampliado*; Instituto Florestal: Sao Paulo, Brazil, 2017; Volume 124, ISBN 3239660180.

57. dos Santos, H.G.; Jacomine, P.K.T.; Dos Anjos, L.H.C.; De Oliveira, V.A.; Lumbreras, J.F.; Coelho, M.R.; de Almeida, J.A.; de Araujo Filho, J.C.; de Oliveira, J.B.; Cunha, T.J.F. *Sistema Brasileiro de Classificação de Solos.*; Embrapa: Brasilia, Brazil, 2018; ISBN 8570358172.
58. FAO. *World Reference Base for Soil Resources 2014. International Soil Classification System for Naming Soils and Creating Legends for Soil Maps*; FAO: Rome, Italy, 2014; ISBN 9789251083697.
59. Mezzalira, S. *Folha Geológica de Piracicaba*; Folha SF-23-M-300; Instituto Geográfico e Geológico do Estado de São Paulo: Sao Paulo, Brazil, 1966.
60. IUSS. *World Reference Base for Soil Resources 2014 Update 2015. International International Soil Classification System for Naming Soils and Creating Legends for Soil Maps*; Food and Agriculture Organization: Rome, Italy, 2015.
61. Oliver, J.E. Monthly precipitation distribution: A comparative index. *Prof. Geogr.* **1980**, *32*, 300–309. [CrossRef]
62. Vrieling, A.; de Jong, S.M.; Sterk, G.; Rodrigues, S.C. Timing of erosion and satellite data: A multi-resolution approach to soil erosion risk mapping. *Int. J. Appl. Earth Obs. Geoinf.* **2008**, *10*, 267–281. [CrossRef]
63. Morton, J.F. The impact of climate change on smallholder and subsistence agriculture. *Proc. Natl. Acad. Sci. USA* **2007**, *104*, 19680–19685. [CrossRef]
64. Almagro, A.; Oliveira, P.T.S.; Nearing, M.A.; Hagemann, S. Projected climate change impacts in rainfall erosivity over Brazil. *Sci. Rep.* **2017**, *7*, 8130. [CrossRef]
65. Goldemberg, J.; Mello, F.F.C.; Cerri, C.E.P.; Davies, C.A.; Cerri, C.C. Meeting the global demand for biofuels in 2021 through sustainable land use change policy. *Energy Policy* **2014**, *69*, 14–18. [CrossRef]
66. Diek, S.; Fornallaz, F.; Schaepman, M.E.; de Jong, R. Barest Pixel Composite for agricultural areas using landsat time series. *Remote Sens.* **2017**, *9*, 1245. [CrossRef]
67. Dogan, H.M.; Kılıç, O.M. Modelling and mapping some soil surface properties of Central Kelkit Basin in Turkey by using Landsat-7 ETM+ images. *Int. J. Remote Sens.* **2013**, *34*, 5623–5640. [CrossRef]
68. Mendes, W.D.S.; Medeiros Neto, L.G.; Demattê, J.A.M.; Gallo, B.C.; Rizzo, R.; Safanelli, J.L.; Fongaro, C.T. Is it possible to map subsurface soil attributes by satellite spectral transfer models? *Geoderma* **2019**, *343*, 269–279. [CrossRef]
69. Shabou, M.; Mougenot, B.; Chabaane, Z.; Walter, C.; Boulet, G.; Aissa, N.; Zribi, M. Soil clay content mapping using a time series of Landsat TM data in semi-arid lands. *Remote Sens.* **2015**, *7*, 6059–6078. [CrossRef]
70. Mannigel, A.R.; Carvalho, M.D.P.E.; Moreti, D.; Medeiros, L.D.R. Fator erodibilidade e tolerância de perda dos solos do Estado de São Paulo. *Acta Sci. -Agron.* **2002**, *24*, 1335–1340. [CrossRef]
71. Carvalho, J.L.N.; Menandro, L.M.S.; de Castro, S.G.Q.; Cherubin, M.R.; Bordonal, R.D.O.; Barbosa, L.C.; Gonzaga, L.C.; Tenelli, S.; Franco, H.C.J.; Kolln, O.T.; et al. Multilocation Straw Removal Effects on Sugarcane Yield in South-Central Brazil. *Bioenergy Res.* **2019**, *12*, 813–829. [CrossRef]
72. Panagos, P.; Borrelli, P.; Meusburger, K.; van der Zanden, E.H.; Poesen, J.; Alewell, C. Modelling the effect of support practices (P-factor) on the reduction of soil erosion by water at European scale. *Environ. Sci. Policy* **2015**, *51*, 23–34. [CrossRef]
73. Carvalho, J.L.N.; Hudiburg, T.W.; Franco, H.C.J.; DeLucia, E.H. Contribution of above- and belowground bioenergy crop residues to soil carbon. *GCB Bioenergy* **2017**, *9*, 1333–1343. [CrossRef]
74. Ruiz Corrêa, S.T.; Barbosa, L.C.; Menandro, L.M.S.; Scarpare, F.V.; Reichardt, K.; de Moraes, L.O.; Hernandes, T.A.D.; Franco, H.C.J.; Carvalho, J.L.N. Straw Removal Effects on Soil Water Dynamics, Soil Temperature, and Sugarcane Yield in South-Central Brazil. *BioEnergy Res.* **2019**, *12*, 749–763. [CrossRef]
75. Conab, Companhia Nacional de Abastecimento. Follow-up of the Brazilian harvest: Sugarcane. Acomp. safra bras. cana, v. 7—Safra 2019/20, n. 3—Terceiro levantamento, Brasília. *Cia. Natl. Abast.* **2020**, *7*, 1–62.
76. Medeiros, G.D.O.R.; Giarolla, A.; Sampaio, G.; Marinho, M.D.A. Diagnosis of the Accelerated Soil Erosion in São Paulo State (Brazil) by the Soil Lifetime Index Methodology. *Rev. Bras. De Ciênc. Do Solo* **2016**, *40*, 1–15. [CrossRef]
77. Bonner, I.J.; Muth, D.J.; Koch, J.B.; Karlen, D.L. Modeled Impacts of Cover Crops and Vegetative Barriers on Corn Stover Availability and Soil Quality. *Bioenergy Res.* **2014**, *7*, 576–589. [CrossRef]
78. Tenelli, S.; Otto, R.; de Castro, S.A.Q.; Sánchez, C.E.B.; Sattolo, T.M.S.; Kamogawa, M.Y.; Pagliari, P.H.; Carvalho, J.L.N. Legume nitrogen credits for sugarcane production: Implications for soil N availability and ratoon yield. *Nutr. Cycl. Agroecosyst.* **2019**, *113*, 307–322. [CrossRef]
79. Rodrigues, W. Valoração econômica dos impactos ambientais de tecnologias de plantio em região de Cerrados. *Rev. Econ. E Sociol. Rural* **2005**, *43*, 135–153. [CrossRef]
80. Bertol, I.; Cogo, N.P.; Schick, J.; Gudagnin, J.C.; Amaral, A.J. Aspectos financeiros relacionados às perdas de nutrientes por erosão hídrica em diferentes sistemas de manejo do solo. *Rev. Bras. De Ciênc. Do Solo* **2007**, *31*, 133–142. [CrossRef]
81. Telles, T.S.; Dechen, S.C.F.; Souza, L.G.A.; Guimarães, M.F. Valuation of soil erosion costs Scientia Agricola. *Sci. Agric.* **2013**, *70*, 209–216. [CrossRef]
82. Telles, T.S.; Guimarães, M.D.F.; Dechen, S.C.F. The Costs of soil erosion. *Rev. Bras. De Ciênc. Do Solo* **2011**, *35*, 287–298. [CrossRef]